PERGAMON

International Journal of Solids and Structures 39 (2002) 1701–1728

INTERNATIONAL JOURNAL OF SOLIDS and STRUCTURES

www.elsevier.com/locate/ijsolstr

On the stiffness characteristics of nonmonolithic elastic structures. Part II. Applications and examples

A. Miettinen *, H. Parland *

Structural Mechanics, Tampere University of Technology, Box 600, FIN-33101 Tampere, Finland

Received 8 September 1999; received in revised form 20 February 2001

Abstract

The theoretical results of Part I [Int. J. Solids Struct. 39, 1673–1699] have been applied to beam and arch structures using a procedure where the nonmonolithic structure is decomposed into an elastic monolithic structure and a rigid body assemblage with partial interpenetration at the joints. Furthermore the indentation of an elastic strip by a rigid punch with various profiles has been analysed by approximate methods. Using the extremum principles concerning the stiffness and the extent of contact, upper and lower bounds of the stiffness characteristics have been determined. © 2002 Elsevier Science Ltd. All rights reserved.

Keywords: Beams; Arches; Joints; Cracks; Contact

1. Introduction

The theoretical results of Part I are applied to contact problems appearing in beam structures, voussoir arches and at indentation of strips. In the following we are mainly concerned with proportional loading. Three basic kinds of behaviour occur in these problems (Fig. 1):

(a) Decreasing contact materializes in preloaded or prestressed ($\sigma_0 \neq 0$) structures where the conforming interfaces ($[r] = 0$) in the initial state are in close contact. Increasing proportional loading P decreases the contact areas.
(b) Increasing contact materializes in structures with nonconforming interfaces ($[r]_n > 0$) and no prestress ($\sigma_0 = 0$). Increasing proportional loading increases the contact area.
(c) Semilinear contact materializes in structures where in the initial unloaded state ($\sigma_0 = 0$) complete contact prevails on all interfaces ($[r] = 0$). At proportional loading the contact areas are discontinuously reduced at the start of loading and remain unchanged thereafter.

* Corresponding authors. Fax: +358-3-365-2811.
E-mail address: antero@junior.ce.tut.fi (A. Miettinen).

PII: S0020-7683(01)00271-2

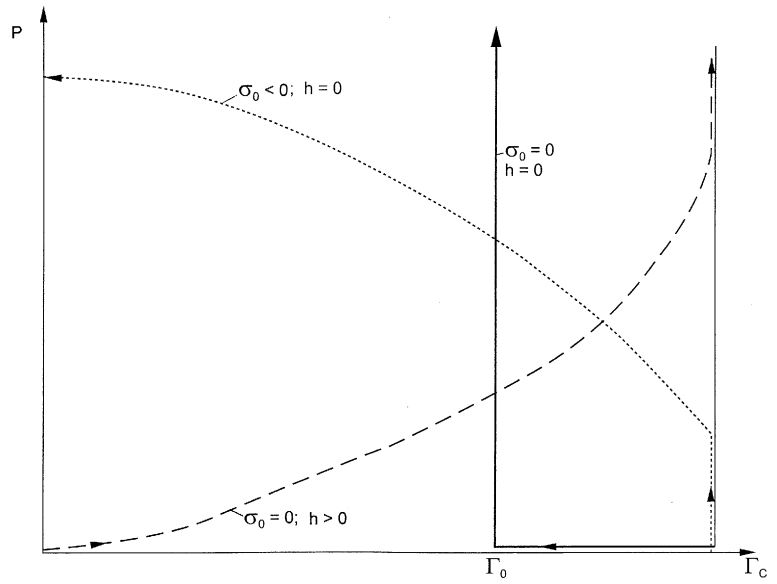

Fig. 1. Load P versus actual contact interface Γ_c. (a) (- - -) Increasing contact. Structure with initial gap ($[r] = h$), no prestress ($\sigma_0 = 0$). (b) (...) Receding contact. Prestressed structure ($\sigma_0 \neq 0$) without initial gaps ($[r] = 0$). (c) (—) Structure without initial gaps ($[r] = 0$) and without prestress ($\sigma_0 = 0$).

Cases (a) and (b) and their combination represent nonlinear contact problems. Cases including semilinear contact provide the simplest way to determine the stiffness characteristics. Based on these solutions, by appropriate modifications, nonlinear cases with nonconforming contact interfaces and prestress have been investigated.

The solutions of contact problems with dissipative friction are not unique. In order to reduce this deficiency special attention is paid to the use of nondissipative geometric friction, that provides unique solutions. The possibilities offered by nondissipative friction have been tested on different structures.

2. Generalized displacements

If the nonmonolithic structure in the initial state is unstressed ($\sigma_0 = 0$) and gapfree ($[r] = 0$), the solution $\{\sigma,\ u\}$ of a boundary value problem corresponding to some load $\{p^*, u^*\}$ can be decomposed into two components

$$\{\sigma,\ u\} = \{\sigma_e, u_e\} + \{\sigma_h, u_h\} \tag{1a}$$

Here $\{\sigma_e, u_e\}$ is the solution of the monolithic elastic structure at the load $\{p^*, u^*\}$. Hence it satisfies all nonhomogeneous load conditions concerning stresses and displacements. $\{\sigma_h, u_h\}$ is the solution of the nonmonolithic structure loaded only by stresses $p_h = p - p_e$ at the joints Γ_c and thus represents the state induced by their edge effect. Generalized displacements can be determined by the equation of virtual work (Part I, Eq. (31)).

$$\int_\Omega \sigma''_{ij}\varepsilon'_{ij}\,d\Omega = \int_{\Gamma_e} \mathbf{p}'' \cdot \mathbf{u}'\,d\Gamma - \int_{\Gamma_c} \mathbf{p}''_{\mu\nu} \cdot \boldsymbol{\gamma}'_{\nu\mu}\,d\Gamma \qquad (\boldsymbol{\gamma}_{\nu\mu} = \boldsymbol{\gamma}_t + \gamma_n \mathbf{n}) \tag{1b}$$

where $\{p'', \sigma''\}$ is an admissible state of equilibrium (AE) and $\{u', \varepsilon', \gamma'\}$ is an admissible kinematic state (AK), Ω denotes the volume, Γ_e the external surface and $\Gamma_c = \cup_r \Gamma_r$ denotes the interfaces of the structure. The generalized displacement U^i of an external surface Γ_j may then be defined by a surface load $p^i = q^i(\Gamma_j)$ corresponding to the generalized load $P^i = 1$ acting on Γ_j. q^i induces in the monolithic structure a state $\{\sigma_e^i, u_e^i\}$. U^i is then determined by a work equation (1b) applied to $\{\sigma_e^i, u_e^i\}$ and $\{\sigma,\ u\}$ giving

$$U^i \cdot 1 = \int_{\Gamma_j} \mathbf{q}^i \cdot \mathbf{u}\, \mathrm{d}\Gamma = \int_{\Omega} \{\sigma_e^i\}^{\mathrm{T}} \{\varepsilon\}\, \mathrm{d}\Omega + \int_{\Gamma_c} \mathbf{p}_e^i \cdot \boldsymbol{\gamma}\, \mathrm{d}\Gamma \tag{2a}$$

Because Betti's rule is valid for monolithic structures and $\boldsymbol{\gamma}_e^i = 0$, we get

$$\int_{\Omega} \{\sigma_e^i\}^{\mathrm{T}} \{\varepsilon\}\, \mathrm{d}\Omega = \int_{\Omega} \{\sigma\}^{\mathrm{T}} \{\varepsilon_e^i\}\, \mathrm{d}\Omega = \int_{\Gamma_e} \mathbf{p} \cdot \mathbf{u}_e^i\, \mathrm{d}\Gamma = \int_{\Gamma_j} \mathbf{q}^i \cdot \mathbf{u}_e\, \mathrm{d}\Gamma \tag{2b}$$

According to Eqs. (2a) and (2b) we obtain

$$U^i = U_e^i + U_h^i \tag{3a}$$

where

$$U_e^i = \int_{\Gamma_j} \mathbf{q}^i \cdot \mathbf{u}_e\, \mathrm{d}\Gamma; \qquad U_h^i = \int_{\Gamma_j} \mathbf{q}^i \cdot \mathbf{u}_h\, \mathrm{d}\Gamma = \sum_r \int_{\Gamma_r} \mathbf{p}_e^i \cdot \boldsymbol{\gamma}\, \mathrm{d}\Gamma \tag{3b}$$

Thus the additional displacement U_h^i equals the work of the $\mathbf{p}_e^i$ in the cracks and joints. In the formula of U_h^i each summation term

$$w_r^i = \int_{\Gamma_r} \mathbf{p}_e^i \cdot \boldsymbol{\gamma}\, \mathrm{d}\Gamma = \int_{\Gamma_r} \mathbf{p}_e^i \cdot (\mathbf{u}_\nu - \mathbf{u}_\mu)\, \mathrm{d}\Gamma = U_{\nu h}^i - U_{\mu h}^i \tag{3c}$$

can be interpreted as locally concentrated discontinuities (which include e.g. mutual translation $v_{\nu\mu}$ and rotation $\omega_{\nu\mu}$) between the members (ν) and (μ), which are deformed according to a solution of the monolithic structure. If the distance between the joints or cracks is small their edge-effects w_r^i will mutually interact, but if the distance is sufficiently large their edge-effects will die away within the intervals. In this case every edge-effect w_r^i reaches an extreme limit value.

Lemma 1. *If only the load p^* is prescribed ($u^* = 0$), complementarity holds and at the supports $\int_{\Gamma_0} \boldsymbol{p} \cdot \boldsymbol{u}\, d\Gamma = 0$, then the states of stress $\{\sigma_e\}$ and $\{\sigma_h\}$ corresponding to a solution $\{u, \sigma\}$ for friction angles ρ, β are orthogonal and the corresponding stress energy $W(\sigma)$ is the sum of the energies $W(\sigma_e)$ and $W(\sigma_h)$*

$$W(\rho, \beta) = W_e + W_h(\rho, \beta) \tag{4}$$

Proof. Expressing the stress energies by symmetric bilinear forms $c(\sigma, \sigma'')/2$ we obtain

$$2W(\sigma_e + \sigma_h) = c(\sigma_e + \sigma_h, \sigma_e + \sigma_h) = c(\sigma_e, \sigma_e) + c(\sigma_h, \sigma_h) + 2c(\sigma_h, \sigma_e) \tag{5}$$

Writing $c(\sigma_h, \sigma_e)$ as a dual pairing $\langle \sigma_h, \varepsilon_e \rangle_H$ we get (Eq. (1b))

$$\langle \sigma_h, \varepsilon_e \rangle_H = \langle p_h, u_e \rangle_{\partial Y} = \langle p_h^0, u_{eB}^0 \rangle_{\partial Y} = 0 \tag{6}$$

because $\gamma_e = 0$ and according to Lemma 1 of Part I, $u_e(\Gamma_e) = u_{eB}^0$ is orthogonal to p_e^0 and $p_e^0 + p_h^0 \in N(B)$. Using the notations $W(\rho, \beta)$, W_e, $W_h(\rho, \beta)$ for $W(\sigma_e + \sigma_h)$, $W(\sigma_e)$, $W(\sigma_h)$, respectively, there follows from Eqs. (5) and (6) the formula (4). □

Applying Eq. (1b) to the states $\{q^i, \sigma^i, \varepsilon^i\} = \{p^*, \sigma_e, \varepsilon_e\}$ and $\{u, \varepsilon, \gamma\}$ induced by the load p^*, we obtain $\langle p^*, u\rangle_Y = \langle p^*, u_e\rangle_Y + \langle p^*, u_h\rangle_Y = \langle \sigma_e, \varepsilon_e\rangle_H + \langle \sigma_e, \varepsilon_h\rangle_H + \langle p_e, \gamma\rangle_{\partial H}$. Because $\langle p^*, u_e\rangle_Y = 2W_e$ and recalling Eq. (6) there follows

$$\langle p^*, u_h\rangle_Y = \langle p_e, \gamma\rangle_{\partial H}; \qquad 2W_h = \langle p - p_e, \gamma\rangle_{\partial H} = \langle p_h, \gamma\rangle_{\partial H} \tag{7}$$

The generalized displacement U_p induced by the load p^* on Γ_e^* is according to Eqs. (3a), (3b) and (7)

$$U_p = U_{pe} + U_{ph} \tag{8a}$$

with

$$U_{pe} = \frac{1}{\|p^*\|}\int_\Omega \{\sigma_e\}^T\{\varepsilon_e\}\,d\Omega; \qquad U_{ph} = \frac{1}{\|p^*\|}\sum_r \int_{\Gamma_r} \mathbf{p}_e\cdot\boldsymbol{\gamma}\,d\Gamma = \sum_r w_r \tag{8b}$$

where w_r is the generalized deformation at the joint (r).

Example. A reinforced concrete beam with vertical cracks has span L, rectangular cross-section $A = td$, reinforcement ratio $\mu = A_a/A$ and carries a load, that induces stresses $\{\sigma_{xc}, \sigma_{yc}, \tau_{xyc}\}$ in the concrete and σ_{xa} in the reinforcement. In the monolithic structure the load induces stresses (with $j = c, a$)

$$\sigma^j_{xe} = n_j\left(\frac{N}{\overline{A}} + \frac{M}{\overline{I}}y\right); \quad \tau_{xye} \cong \frac{3Q}{2\overline{A}}\left(1 - \left(\frac{2y}{d}\right)^2\right); \quad \sigma_{ye} \cong \frac{3p_y}{4t}\left(\frac{2y}{d} - \frac{1}{3}\left(\frac{2y}{d}\right)^3\right) \tag{9}$$

where $\overline{A} = A(1 + n_a\mu)$, $\overline{I} = I(1 + n_a\sum(y_a/i)^2)$, $n_a = E_a/E_c$, $n_c = 1$, $\mu = A_a/A$ and p_y is the distributed transversal load. The generalized elongation $v(L)$ of the centroidal axis is, with $\sigma^i_e = n_jN/\overline{A}$ induced by $N = 1$, according to formulae (2a), (2b) and (3a)–(3c)

$$1\cdot v(L) = \int_0^L \int_A \frac{n_j}{\overline{A}}u_x\,dA = v_e + \sum_k \int_{A_k}\frac{\sigma^i_e\gamma_{nk}}{\overline{A}}\,dA = \int\frac{N}{E\overline{A}}dA + \sum_k\frac{V_{hk}}{\overline{A}}; \quad (n_j = \{n_a, n_c\}) \tag{10a}$$

The generalized mutual rotation $\omega(L)$ of the endfaces of the beam is, with $\sigma^i_e = yn_jM/\overline{I}$ induced by $M = 1$, accordingly

$$1\cdot\omega(L) = \int_0^L \sum_j \int_A \frac{n_jy}{\overline{I}}u_x\,dA = \omega_e + \sum_k\int_{A_k}\frac{\sigma^i_e\gamma_{nk}}{\overline{I}}\,dA = \int\frac{M}{E\overline{I}}dA + \sum_k\frac{y_{hk}V_{hk}}{\overline{I}} \tag{10b}$$

where V_h and y_hV_h are the crack-volume and its moment with regard to the elastic centroid-axis, respectively. Because $V_h \geqslant 0$ Eq. (10a) implies, that in a beam under pure bending cracking always induces an extension of the centroid-axis, even if the cracks do not reach the axis in question.

3. The stiffness characteristics of a rectangular panel

A rectangular elastic panel (1) with depth d, length $l = 2d$ and cross-section $A = td$ is pressed against a rigid wall (0) at $x = 0$ by forces $\{R_i\}^T = \{N, Q, M\}^T$ at $x = l$ (Fig. 2). If the panel is a part of a beam, the edge effect of the dry joint at $x = 0$ will die away at distance $x \geqslant d$ from the support. Therefore the load stresses $\mathbf{p}^*$ acting at cross-section $x = l$ are (Miettinen, 1988)

$$\mathbf{p}^* = \sum_i \mathbf{q}^iR_i = \left(\frac{N}{A} + \frac{M(l)}{I}y\right)\mathbf{i} + \frac{3Q}{2A}\left(1 - \left(\frac{2y}{d}\right)^2\right)\mathbf{j} \tag{11a}$$

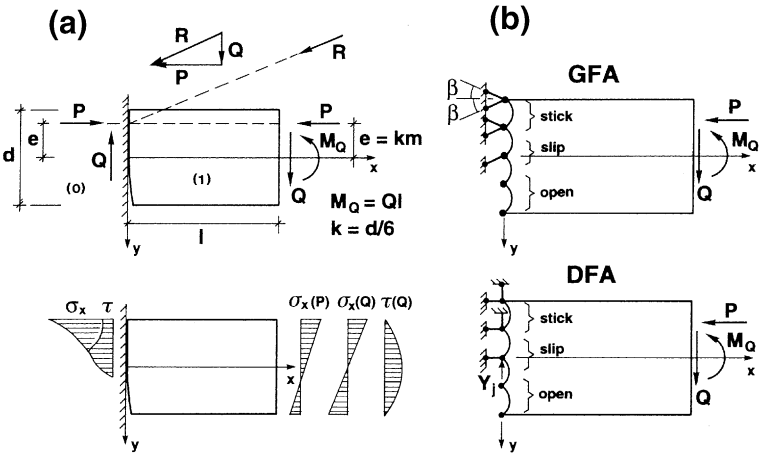

Fig. 2. (a) Eccentrically loaded panel. (b) Kinematics and reactions at the support according to nondissipative (GFA) and dissipative (DFA) friction.

where

$$\mathbf{q}^1 = \frac{1}{A}\mathbf{i}; \quad \mathbf{q}^2 = \frac{3}{2A}\left(1 - \left(\frac{2y}{d}\right)^2\right)\mathbf{j}; \quad \mathbf{q}^3 = \frac{y}{I}\mathbf{i} \ \ (I = Ad^2/12) \tag{11b}$$

Let at load $\mathbf{p}^*$ the state $\{\sigma_e, u_e\}^T$ be the solution for the clamped monolithic beam and the state $\{\sigma,\ u\}^T$ be the solution for the nonmonolithic structure. According to the complementarity rule (Eq. (42), Part I) and Eq. (2b) the generalized displacements at $x = l$, $\{U^i(l)\} = \{\int \mathbf{q}^i(y) \cdot \mathbf{u}(l,y)\,\mathrm{d}A\}$, induced by $\mathbf{p}^*$ are

$$U^1 = U_x(l) = \frac{1}{A}\int_A u_x\,\mathrm{d}A; \quad U^2 = U_y(l) = \frac{3}{2A}\int_A (1-(2y/d)^2)u_y\,\mathrm{d}A; \quad U^3 = \vartheta(l) = \frac{1}{I}\int_A y u_x\,\mathrm{d}A \tag{12a}$$

where U_x, U_y represent translations and ϑ represents a rotation. These U^i linearize the displacement $\mathbf{u}(l,y)$ into

$$\bar{\mathbf{u}}(l,y) = (U_x(l) + \vartheta(l)y)\mathbf{i} + U_y(l)\mathbf{j} \tag{12b}$$

The projection of the linearized displacement of the point of action of $\mathbf{R} = -P\mathbf{i} + Q\mathbf{j}$ on the direction of $\mathbf{R}$ is

$$U_R(l) = U^4 = ((-U_x(l) + \vartheta(l)\mathrm{e}(l))P + U_y(l)Q)/|\mathbf{R}| \tag{13a}$$

where $e(l) = -y_p$ is the eccentricity of P at $x = l$. $U_R(l)$ can then be expressed by the resultant $\mathbf{R}$ or by the compressive force P and a deformation parameter $\delta(m,q)$

$$U_R = \frac{|\mathbf{R}|d}{EA}\delta(m,q) = \frac{Pd}{EA}\delta(m,q)(1+q)^{1/2} \tag{13b}$$

where $m = e(0)/k$; $q = Q/P$ and $k = d/6$ (Fig. 3). The stiffness is then defined by

$$D(\mathbf{R},\rho,\beta) = \frac{|\mathbf{R}|}{U_R} = \frac{EA}{\delta d} \tag{13c}$$

By computing $U_e^i(l)$ of the monolithic clamped cantilever with $\boldsymbol{\gamma}_{10} = \mathbf{u}_e(0,y) = 0$ and $U^i(l)$ of the nonmonolithic structure with $\boldsymbol{\gamma}_{10} = \mathbf{u}(0,y) \neq 0$ on Γ_c, we obtain by subtraction $U_h^i = U^i(l) - U_e^i(l)$ the displacement caused by the deformation $\boldsymbol{\gamma}_{10}$ on Γ_c: $U_{xh}(l) = U_x(l) - U_{xe}(l) = v_{xh}(l)$; $U_{yh}(l) = U_y(l) - U_{ye}(l) = v_{yh}(l)$;

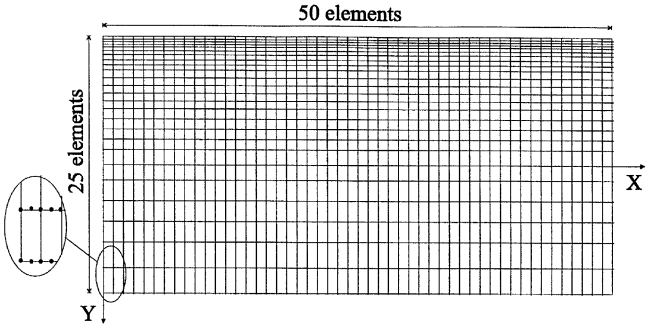

Fig. 3. Element mesh used.

$\vartheta_h(l) = \vartheta(l) - \vartheta_e(l)$; $U_{Rh}(l) = U_R(l) - U_{Re}(l)$. The corresponding generalized deformations at the support $w^i(0) = U^i(0) - U^i_e(0) = \int_{\Gamma_c} \mathbf{p}^i_e \cdot \boldsymbol{\gamma}_{10}\, d\Gamma$ are thus

$$w^1(0) = v_{xh}(0) = U_{xh}(l); \quad w^2(0) = v_{yh}(0) = U_{yh}(l) - l\omega_h(0); \quad w^3(0) = \omega_h(0) = \vartheta_h(l); \quad w^4 = U_{Rh} \tag{14a}$$

because $U^i_e(0)$, $u^i_e(0) = 0$. The $w^i(0)$ define a linearized deformation $\overline{\boldsymbol{\gamma}}_{10}$ at the support

$$\overline{\boldsymbol{\gamma}}_{10} = (v_{xh}(0) + \omega_h(0)y)\mathbf{i} + v_{yh}(0)\mathbf{j} \tag{14b}$$

The generalized deformations of the joint can be expressed by the compressive force P, the deformation parameters α_h, η_h, ε_h, δ_h and the ratios $m = 6e(0)/d$, $q = Q/P$

$$v_{xh}(0) = \frac{Pd}{EA}\eta_h(m,q); \qquad v_{yh}(0) = \frac{Pd}{EA}\varepsilon_h(m,q) \tag{15a}$$

$$\omega_h(0) = \frac{Pd}{EAk}\alpha_h(m,q); \qquad U_{Rh} = \frac{Pd}{EA}\delta_h(m,q)\sqrt{1+q^2} \tag{15b}$$

These deformations correspond to the limit state of free contact and they are independent of the length l—if l is large enough ($l > d$).

A comparison was made between the geometric friction solutions (GFA) with friction angles $\varphi = \beta = \pi/4$ and dissipative friction solutions (DFA) with $\varphi = \rho = \pi/4$ and Poisson's ratio $\nu = 0.2$. The computations were carried out by the finite element method (Fig. 3) for different eccentricities m and different ratios q. The support conditions were realized by very stiff bars (Fig. 2b), which were "removed" (by reducing their stiffness sufficiently) as needed during the iteration process. In the case of nondissipative friction at each iteration cycle all the bars in tension were removed until the state ("removed/not") of any of the bars did not change. In the case of dissipative friction the horizontal bars were also removed when in tension (force $X_j > 0$, open region). Instead a vertical bar was removed if it was in the open region or if its force Y_j was larger than the friction allowed ($|Y_j| > |X_j| \tan\varphi$, slip region) or if it had been in the region of slip in the previous iteration cycle. In the slip region the removed vertical bars were replaced by forces $Y_j = \mathrm{sign}(u_{yj})|X_j| \tan\varphi$ and during the next cycle it was checked that the displacement u_{yj} did not change sign; if it did, the very stiff vertical bar was restored. The iteration was continued until the state of any of the bars did not change and the changes in all the forces Y_j became negligible. Therefore the DFA-solution requires considerably more computation time than the GFA-solution.

The results of the computation (Figs. 4 and 5) show that the deformation parameter δ_h(DFA) almost coincides with δ_h(GFA) but in accordance with the maximum property of the GFA-stiffness δ_h(GFA) $<$ δ_h(DFA). Also ε_h(DFA) coincides closely with ε_h(GFA), but α_h(GFA) and η_h(GFA) are smaller than

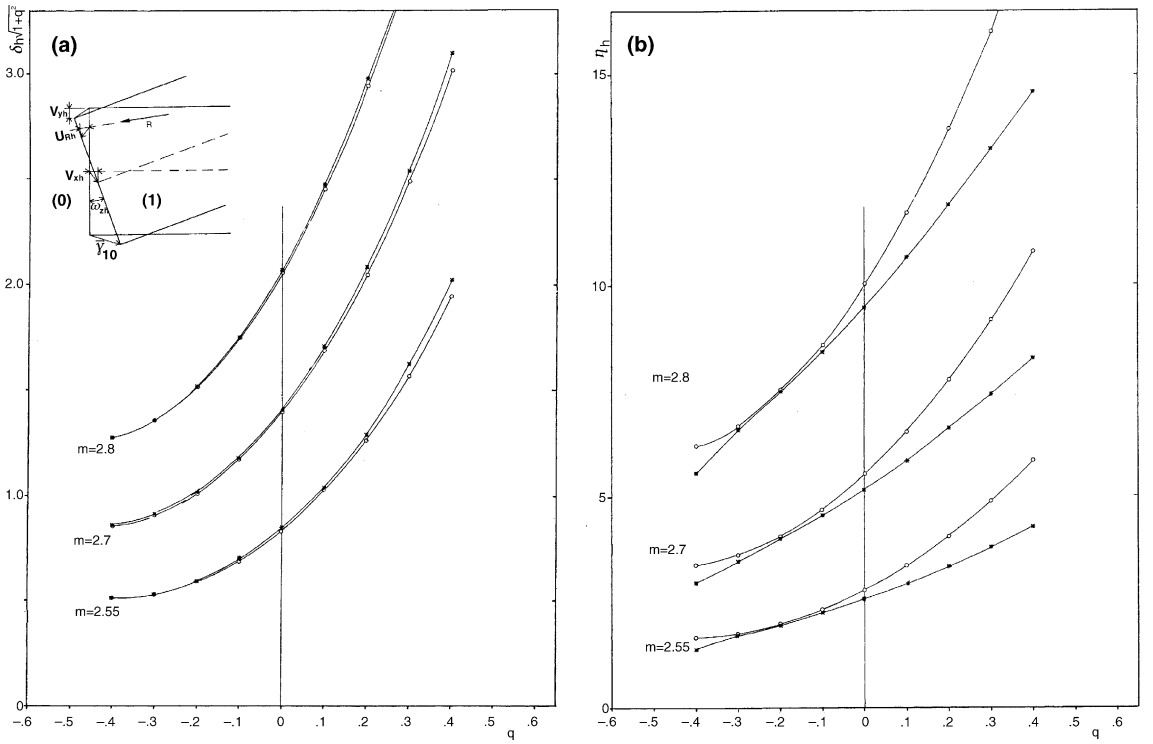

Fig. 4. Parameters of generalized joint deformations. (a) Stiffness parameters δ_h of U_{Rh}. (b) Dilatation parameters η_h of v_{xh}, $\tan\varphi = 1$, (---○---) GFA solution, (---✱---) DFA solution.

α_h(DFA) and η_h(DFA), respectively, especially if $\text{sign}(m) = \text{sign}(q)$. On the other hand if $\text{sign}(m) = -\text{sign}(q)$, and consequently the resultant R remains within the panel, the difference does not exceed 10%. This case corresponds to thrust lines within masonry and concrete structures.

4. Contact mechanics of the voussoir arch

We consider an elastic voussoir arch with fixed abutments. Special attention is paid to the stiffness characteristics of the arch. The connection of this theory with the theory of the monolithic arch and the linear theory of stability of arches with rigid voussoirs is analysed.

We recapitulate those points of the linear theory of stability, which we shall need in the sequel

(a) The displacements u are small and do not change the equilibrium.
(b) The voussoirs are rigid and have infinite strength.
(c) The joints do not transfer tensile stresses ($\sigma \leqslant 0$).
(d) The interfaces between the blocks are conforming planes and their normal **n** coincides with the direction of the centroid axis of the arch (Fig. 6).
(e) Because of sufficient friction at the joints contact sliding is excluded, $\gamma_t = 0$, and the gap deformation can be expressed by the dilatation

$$\gamma_n = v + \omega y \tag{16}$$

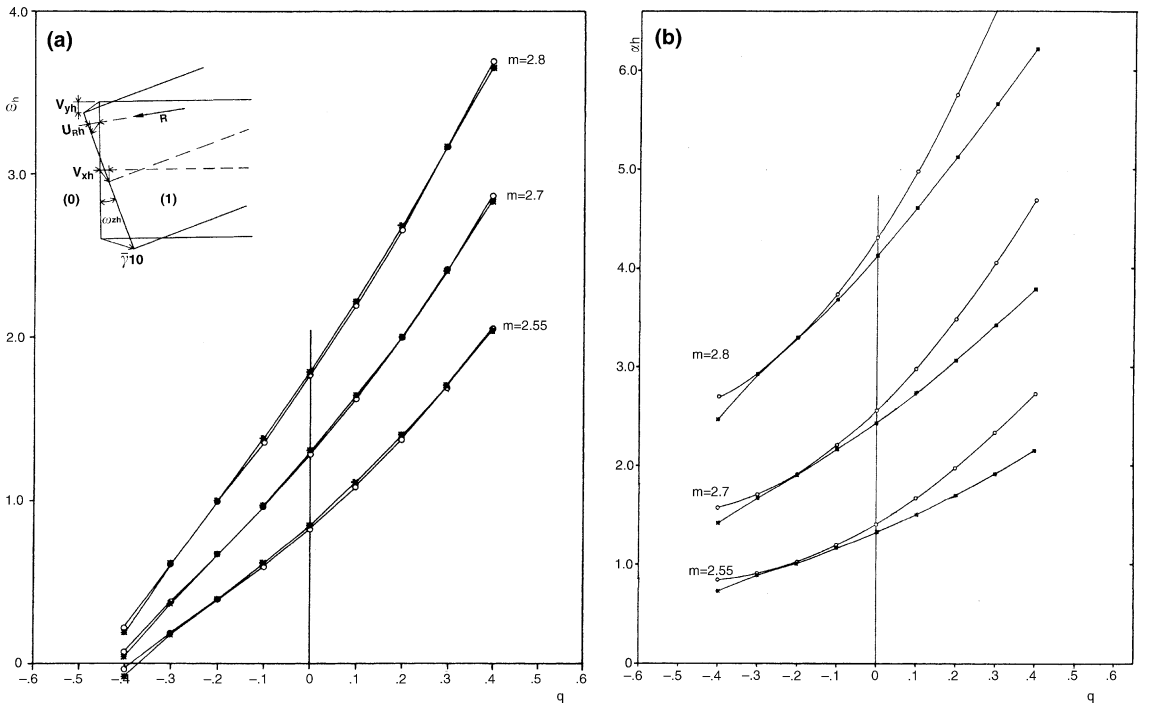

Fig. 5. Parameters of generalized joint deformations. (a) Shear parameters ε_h of v_{yh}. (b) Rotation parameters α_h of ω_h, $\tan\varphi = 1$, (---○---) GFA solution, (---✱---) DFA solution.

where v denotes the dilatation of the centroid axis and ω the mutual rotation of the end faces.

(f) The noninterpenetration requires that $v + \omega y \geqslant 0$ for any $y \in A_{\mu\nu}$. Therefore, if contact between the voussoirs is to be retained the axis of rotation is situated either on the extrados or the intrados ($y = \{-c^-, c^+\}$). Thus, a displacement field $\{u\}$ with preserved contact between the voussoirs is possible only if the arch is transformed into a hinge mechanism. To this corresponds a neutral state of equilibrium represented by a linear arch S_n that passes through the hinges of the mechanism. The mechanism and the linear arch S_n define together the limit state of collapse.

The set of loads P, to which corresponds admissible equilibrium, constitutes the convex cone $E(P)$ of stability in the load space R^m. The generatrices P^n of the lateral surface of $E(P)$ are orthogonal to the set of load displacements U^n of the collapse mechanism. These U^n in turn constitute the generatrices of the convex cone $\Xi(U)$ of detachment. The interior $\Xi^0(U)$ of $\Xi(U)$ constitutes the cone of disintegration (Fig. 7c).

We base the analysis of the elastic voussoir arch on the following assumptions:

(i) No contact slidings occur at the joint, $\gamma_t = 0$ where $\sigma_s \neq 0$.
(ii) The joints do not transfer tensile stresses $\sigma_s \leqslant 0$.
(iii) The shear force $Q(s)$ is small compared with the compressive force $-N(s)$:$|Q| \ll |N|$.

The state of stress and strain $\{\sigma,\ u\}$ induced by some load $\{P\}$ is decomposed according to Section 2

$$\{\sigma,\ u\} = \{\sigma_e, u_e\} + \{\sigma_h, u_h\} \tag{17}$$

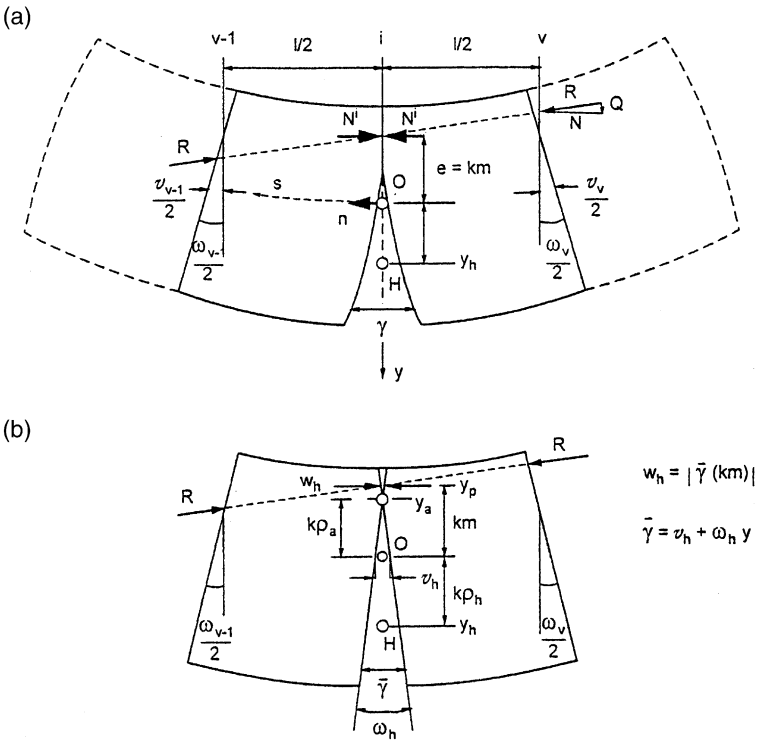

Fig. 6. Deformation of two adjacent voussoir halves. (a) Actual configuration. (b) Linearized decomposed configuration.

where $\{\sigma_e, u_e\}$ corresponds to a monolithic elastic arch. Neglecting the curvature of the monolithic arch, the longitudinal strains ε_{se} and stresses σ_{se} are thus

$$\varepsilon_{se} = \varepsilon_0(s) + \dot{\omega}(s)y; \qquad \sigma_{se} = \frac{N(s)}{A} + \frac{M(s)y}{I} \tag{18}$$

$\{\sigma_h, u_h\}$ is a state of eigenstress induced by the edge effect of the opening gaps of the joints and is orthogonal to $\{\sigma_e, u_e\}$ ($\langle\sigma_h, \varepsilon_e\rangle = 0$). Therefore the stress energy W_σ can be expressed as the sum of two orthogonal parts

$$W(\sigma) = W_e(\sigma_e) + W_h(\sigma_h) \tag{19}$$

Because dissipative work is excluded, Castigliano's rule and Maxwell's rule expressed by the derivatives of W, Clapeyron's equation, and the extremum principles of stiffness remain valid. The multiplicity rule applies also to the elastic voussoir arch. If the load $\{P\}$ induces a state $\{\sigma,\ u\}$, then the load $\{\lambda P\}$, where $\lambda > 0$, induces a state $\{\lambda\sigma, \lambda u\}$ with unchanged contact interfaces at the joints and unchanged linear arch S.

In order to adapt the treatment of the voussoir arch to that of the monolithic arch, we consider an assemblage of two adjacent voussoir halves (Fig. 6a). The elongation $\Delta u_s(y)$ of the assemblage can be expressed by

$$\Delta u_s(y) = u_v - u_{v-1} = v + \omega y \tag{20}$$

where v is the extension of the centroid axis and ω denotes the mutual rotation of the end faces A_{v-1} and A_v. If we decompose the displacement field $\{u_s, u_y\}$ considering the joint i as a plane of symmetry with symmetrical $\{u_s, u_y\}_s$ induced by N^i and antisymmetrical $\{u_s, u_y\}_a$ induced by the shearforce Q, the latter one may not affect the distance Δu_s of symmetrically situated points (Lemma B.2, Appendix B). This implies

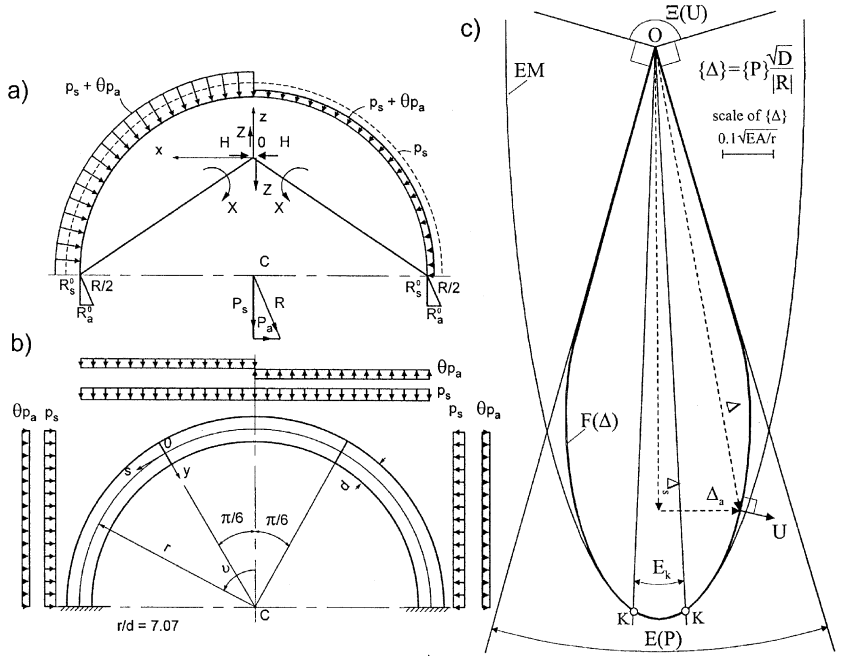

Fig. 7. Semicircular arch, that comprises three voussoirs. (a) Loading, redundants and reactions. (b) Elevation. (c) Stiffness surface $F(\Delta)$, stiffness ellipsoid $\mathrm{EM}(\Delta)$, cone of monolithic kern $E_k(P)$, cone of stability $E(P)$ and cone of detachment $\Xi(U)$.

that $\Delta u_s(y)$ corresponds to a displacement field, where according to Fig. 6b the endfaces and the contact faces of the assemblage remain plane.

Let the dimensions of the voussoir be length l, depth d and cross-section A. The effect of the curvature is overlooked in the following. The generalized deformations v and ω are determined according to Section 2 by using elastic states $\{\sigma'_e, \varepsilon'_e\}$ and $\{\sigma''_e, \varepsilon''_e\}$ induced by a constant normal force $N' = 1$ and constant bending moment $M'' = 1$, respectively, applied to the monolithic straight segment ($\gamma_n = 0$)

$$\sigma'_{se} = \frac{1}{A}; \quad \sigma'_{ye} = \tau'_{sye} = \gamma'_{sye} = 0; \qquad \varepsilon'_{se} = \frac{1}{EA}; \quad \varepsilon'_{ye} = -\frac{v}{EA} \tag{21}$$

$$\sigma''_{se} = \frac{y}{I}; \quad \sigma''_{ye} = \tau''_{sye} = \gamma''_{sye} = 0; \qquad \varepsilon''_{se} = \frac{y}{EI}; \quad \varepsilon''_{ye} = -\frac{vy}{EI} \tag{22}$$

Proceeding according to Section 2 (Eqs. (2a) and (2b), (3a) and (3b)) we get the work equations

$$\begin{aligned} 1 \cdot v &= \int_A \sigma'_{se} \Delta u_s \, \mathrm{d}A = \int_1 \int_A \sigma'_{se} \varepsilon \, \mathrm{d}A \, \mathrm{d}s + \int_{Ai} \sigma'_{se} \gamma_n \, \mathrm{d}A \\ &= \int_1 \int_A \frac{1}{EA} \sigma_s \, \mathrm{d}A \, \mathrm{d}s - v \int_1 \int_A \frac{1}{EA} \sigma_y \, \mathrm{d}A \, \mathrm{d}s + \int_{Ai} \frac{\gamma_n \mathrm{d}A}{A} \cong \int_1 \frac{N \, \mathrm{d}s}{EA} + \int_{Ai} \frac{\gamma_n \mathrm{d}A}{A} \end{aligned} \tag{23}$$

$$\begin{aligned} 1 \cdot \omega &= \int_A \sigma''_{se} \Delta u_s \, \mathrm{d}A = \int_1 \int_A \sigma''_{e} \varepsilon \, \mathrm{d}A \, \mathrm{d}s + \int_{Ai} \sigma''_{se} \gamma_n \, \mathrm{d}A \\ &= \int_1 \int_A \frac{y}{EI} \sigma_s \, \mathrm{d}A \, \mathrm{d}s - v \int_1 \int_A \frac{y}{EI} \sigma_y \, \mathrm{d}A \, \mathrm{d}s + \int_{Ai} \frac{y \gamma_n \mathrm{d}A}{I} \cong \int_1 \frac{M \, \mathrm{d}s}{EI} + \int_{Ai} \frac{y \gamma_n \mathrm{d}A}{I} \end{aligned} \tag{24}$$

Because of condition (iii), the terms with σ_y have been be neglected. The first integrals to the right express the elongation of the centroid axis $\Delta u(0)_e = v_e$ and the rotation ω_e, respectively, of the monolithic voussoir ($\gamma_n = 0$). $\int \gamma_n \, dA = V_h$ represents the gap volume and $\int y\gamma_n \, dA = y_h V_h$ represents its moment. For the extension $\Delta u_s(y)$ the Eqs. (23) and (24) provide a linearized decomposition according to Eq. (20)

$$\Delta u_s(y) = \Delta u(y)_e + \Delta u(y)_h; \quad \Delta u(y)_e = v_e + \omega_e y; \quad \Delta u(y)_h = v_h^i + \omega_h^i y = \overline{\gamma}^i \tag{25}$$

where $v_e = \int_l (N/EA)\, ds$, $\omega_e = \int_l (M/EI)\, ds$, $v_h^i = V_h/A$, $\omega_h^i = y_h V_h/I$. $\Delta u_h(y)$ represents the linearized gap deformation $\overline{\gamma}^i$ at joint (i). Thus we arrive at the configuration of Fig. 6b. The blocks deform according to Navier's assumption and adjacent endfaces experience a mutual rotation ω_h^i around a hinge (a) with ordinate y_a within the cross-section in the interval $[k, e]$, where k is the kern point distance of the cross-section.

We assume that v_h^i and ω_h^i together with the interpenetration w_{ph}^i at level $y_p^i = M^i/|N^i|$ depend solely on local $N(s^i)$ and $M(s^i)$ at joint (i). According to the multiplicity rule the v_h^i, ω_h^i and $w_{ph}^i = -\Delta u_h(e^i)$ at given eccentricity $e^i = -y_p^i$ of $|N^i|$ are proportional to $|N^i|$. In the limit case of free contact, where stress-singularities do not occur, v_h^i, ω_h^i and w_{ph}^i can be expressed by

$$v_h^i = \frac{|N^i|d}{EA}\eta_h(m^i, \lambda); \quad \omega_h^i = \frac{|N^i|d}{EAk}|\alpha_h(m^i, \lambda)|\operatorname{sign} M^i; \quad w_{ph}^i = \frac{|N^i|d}{EA}\delta_h(m^i, \lambda) \tag{26}$$

where $m^i = e^i/k$ and $\lambda = 1/d$. Because $M^i = |N^i|e^i$ and $w_{ph}^i = e^i\omega_h^i - v_h^i$ and Eq. (26), there applies

$$\delta_h = m\alpha_h - \eta_h > 0; \quad \alpha_h = \frac{1}{2}\frac{\partial \delta_h}{\partial m}; \quad \rho_h = \frac{y_h}{k} = \frac{c\alpha_h}{k\eta_h}; \quad \rho_a = -\frac{y_a}{k} = \frac{\eta_h}{\alpha_h} \tag{27}$$

where c is the edge distance and δ_h, η_h are nonnegative. If $|m| \leqslant 1$ then δ_h, η_h, $\alpha_h = 0$ and if $|m| \to |c/k|$ then δ_h, $|\alpha_h|$, $\eta_h \to \infty$. In order to extract the edge effects v_h, ω_h, w_h and y_h, y_a for a voussoir with variable N, M we resort to the field $\{u, \varepsilon, \gamma\}$ of symmetrically loaded ($Q = 0$) straight voussoirs where at the joints τ^i, $\gamma_t^i \cong 0$. Since Clapeyron's equation is valid and $|\Delta u_h(y_p)| = w_h^i$ we get, neglecting the effect of shearforce Q and transversal loads, using Eq. (26)

$$\begin{aligned} &2W_h^i = |N^i|\Delta u_h(e^i) = |N^i|w_{ph}^i = \frac{(N^i)^2 d}{EA}\delta_h(m^i, \lambda); \\ &\frac{\partial W_h^i}{\partial N^i} = \frac{|N^i|d}{EA}\eta_h(m^i, \lambda) = v_h^i; \quad \frac{\partial W_h^i}{\partial M^i} = \frac{|N^i|d}{EAk}\alpha_h(m^i, \lambda) = \omega_h^i \end{aligned} \tag{28}$$

For a voussoir with rectangular cross-section $A = bd$, approximate expressions of δ_h, η_h, α_h including four limit cases have been determined. Usually $\lambda > 1$ and in this case δ_h, η_h, α_h attain limit values not depending on λ. The following approximations are used (Parland, 1995)

$$\begin{aligned} &\delta_h \cong \sqrt{r}(1 - (|m| - 2)^2)^r \frac{(|m| - 1)^3}{3(3 - |m|)}; \quad \eta_h \cong \frac{(3 + r(2 - |m|)|m|)\delta_h}{1 - (|m| - 2)^2}; \\ &|\alpha_h| \cong \frac{(4 - |m| + r(2 - |m|))\delta_h}{1 - (|m| - 2)^2} \end{aligned} \tag{29}$$

where $r = 0.55$.

The above deductions imply that the state $\{\sigma,\ u\}$ of the arch can be decomposed into a monolithic part $\{\sigma_e, u_e\}$ with a continuous displacements field u_e and stresses σ_e of the monolithic arch according to Navier's rule, and a nonmonolithic part $\{\sigma_h, u_h\}$ characterized by discrete linear discontinuities $\overline{\gamma}_n$ at the joints with hinges within the cross-sections. The voussoir arch is thus kinematically decomposed into a monolithic elastic arch AR_e and a pseudo arch AR_h with rigid voussoirs and discrete hinges at some joints. These structures are connected by the same linear arch S. Therefore neither of them separately complies

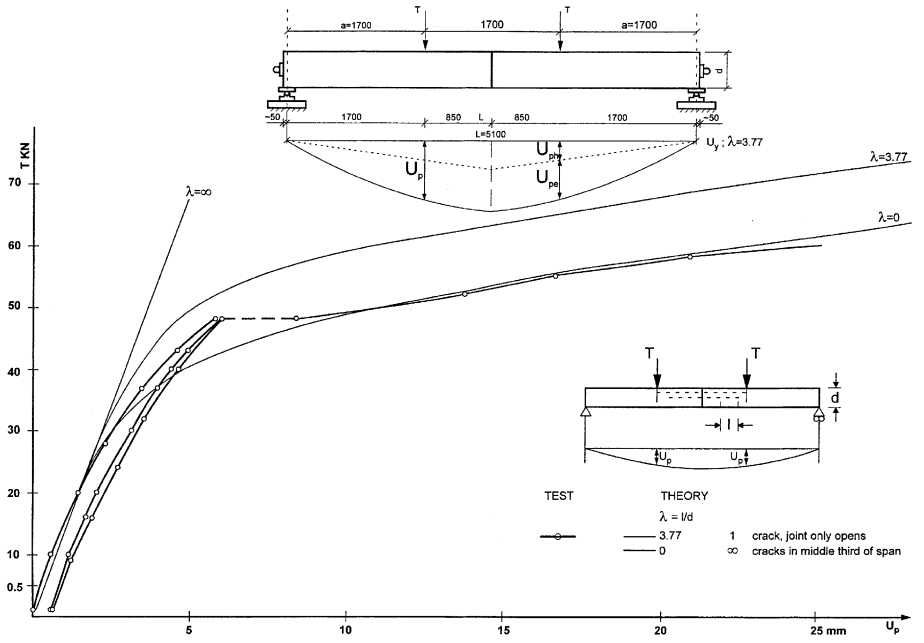

Fig. 8. Prestressed granite beam; load–deflection u_p.

with the conditions of fixed abutments. The equilibrium of the AR_e does not coincide with that of the original clamped monolithic arch AR_e^0.

The equilibrium of the arch is determined by three redundants, the horizontal thrust H, the shear force Z and moment X which act at the elastic centroid of the arch (Fig. 7a). These determine together with the nonredundant N^0, M^0 the normal force N and moment M

$$\begin{aligned} N(s) &= N^0 - H\cos\vartheta - Z\sin\vartheta; \quad N = \int_A \sigma \,\mathrm{d}A \\ M(s) &= M^0 - Hz - Zx + X; \quad M = \int_A \sigma y \,\mathrm{d}A \end{aligned} \tag{30}$$

where $z(s)$ denotes the ordinate of the axis of the arch and $\cos\vartheta = \mathrm{d}x/\mathrm{d}s$.

An analysis of the arch according to the force method is based on the minimum condition of the stress energy W_σ. According to Eq. (19) W_σ can be expressed as the sum of W_e of the monolithic arch and the sum $\sum W_h^i$ of the stress energies induced by the opening of joints

$$W_\sigma = \frac{1}{2}\int_0^L \left(\frac{N^2}{EA} + \frac{M^2}{EI}\right)\mathrm{d}s + \frac{1}{2}\sum_i \frac{(N^i)^2 d}{EA}\,\delta_h(m^i,\lambda) \tag{31}$$

The solution with respect to the redundants corresponding to fixed abutments is obtained by

$$\frac{\partial W_\sigma}{\partial H} = \frac{\partial W_e}{\partial H} + \frac{\partial W_h}{\partial H} = 0; \quad \frac{\partial W_\sigma}{\partial Z} = \frac{\partial W_e}{\partial Z} + \frac{\partial W_h}{\partial Z} = 0; \quad \frac{\partial W_\sigma}{\partial X} = \frac{\partial W_e}{\partial X} + \frac{\partial W_h}{\partial X} = 0 \tag{32}$$

where the derivatives of W_e and W_h represent the mutual translations v_{ex}, v_{hx} and v_{ez}, v_{hz} and rotations ω_e, ω_h of the abutments, respectively (Fig. 7a). Inserting M and N from Eq. (30) and applying Eqs. (31) and (32), substitution with $I = Ai^2$ gives

$$
\begin{aligned}
H\left(\int_L \frac{1}{EA}\left(\cos^2\vartheta + \left(\frac{z}{i}\right)^2\right)\mathrm{d}s\right) &= \int_L \left(\frac{N^0\cos\vartheta}{EA} + \frac{M^0 z}{EI}\right)\mathrm{d}s + \sum_i \frac{|N^i|d}{EA}\left(\eta_{\mathrm{h}}^i\cos\vartheta + \frac{z^i}{k}\alpha_{\mathrm{h}}^i\right)\\
Z\left(\int_L \frac{1}{EA}\left(\sin^2\vartheta + \left(\frac{x}{i}\right)^2\right)\mathrm{d}s\right) &= \int_L \left(\frac{N^0\sin\vartheta}{EA} + \frac{M^0 x}{EI}\right)\mathrm{d}s + \sum_i \frac{|N^i|d}{EA}\left(\eta_{\mathrm{h}}^i\sin\vartheta + \frac{x^i}{k}\alpha_{\mathrm{h}}^i\right) \qquad (33)\\
X\left(\int_L \frac{\mathrm{d}s}{IE}\right) &= -\int_L \frac{M^0\mathrm{d}s}{EI} - \sum_i \frac{|N^i|d}{EAk}\alpha_{\mathrm{h}}^i
\end{aligned}
$$

If the sums on the right sides of the equations are zero, we get the well-known equations for the monolithic arch $\mathrm{AR}_{\mathrm{e}}^0$ with fixed abutments. From the Eq. (33) we can iteratively solve the unknowns H, Z and X. Because of the strong and progressive nonlinearity (as function of eccentricity $m^i(H,Z,X)$) of the terms containing η_{h}^i, α_{h}^i on the right side of Eq. (33), an iteration process with gradually increasing underrelaxation (as function of m^i and oscillations observed in the solution process) has been used. As starting point for the iteration process the solution of the monolithic structure (which we get using $m^i = 0$, and $\eta_{\mathrm{h}}^i = \alpha_{\mathrm{h}}^i = 0$, on the right side of the Eq. (33)) or, when solving for several gradually changing loading-cases, the solution of a previous loading-case have been used with success.

The following limit-case modes can be derived from the above equations:

(a) If a set of loads $\{P_{\mathrm{k}}\}$ induces solutions, where at every joint $|m| < 1$, the sums on the right of Eq. (33) are zero and the arch behaves monolithically. The set $\{P_{\mathrm{k}}\}$ constitutes, because of the superposition law, in R^n a convex cone E_{k}, the cone of the monolithic kern of the arch.
(b) If the load P induces a linear arch S which approaches the intrados and extrados c^i, the hinges (y_{a}^i) approach gradually the points (y_{p}^i) of action of S within A^i. Thus, if $|e^i| \to |c^i|$ then $|y_{\mathrm{a}}^i| \to |c^i|$ and δ_{h}, η_{h}, $|\alpha_{\mathrm{h}}| \to \infty$ and the sums of the right members of Eq. (33) begin to dominate over the integrals. Since $|\rho_{\mathrm{a}}^i| \to |m^i| \to |c^i/k|$ (Eq. (27)), the displacement field approaches that of a rigid body mechanism.

The behaviour of the arch can be given a more transparent interpretation by the stiffness D, the stiffness vector Δ, and stiffness surface $F(\Delta)$. According to Eq. (19) and Part I, Eq. (59b) there applies

$$
D''_\sigma = \frac{|P|^2}{2W''_\sigma} = \frac{|P|^2}{2W''_{\mathrm{e}} + 2W''_{\mathrm{h}}} \qquad (34)
$$

Every iteration step, that corresponds to an admissible state AE, provides a lower bound D''_σ to D, where the kinematical conditions at the abutments are violated. The stiffness vector Δ and the stiffness surface $F(\Delta)$ are defined by (Part I, Eqs. (65a) and (66))

$$
\Delta_i = D^{1/2}P_i/|P|; \quad F(\Delta) = 2W_\sigma(\Delta) - 1 = 0 \qquad (35)
$$

The stiffness surface $F(\Delta)$ is contained in the cone of stability $E(P)$, and $F(\Delta)$ and $E(P)$ have a common origin at the apex of the cone $E(P)$. The load–displacement U is orthogonal to $F(\Delta)$. In addition:

(a') If the load P is within the cone of the monolithic kern E_{k} the $F(\Delta)$ coincides with the stiffness ellipsoid $\mathrm{EM}(\Delta)$ of the monolithic arch (Proposition 3, Part I).
(b') Immediately outside E_{k} is a region of $\{\Delta\}$ where $F(\Delta)$ closely follows $\mathrm{EM}(\Delta)$ inside the ellipsoid, that forms an osculating surface of $F(\Delta)$.
(c') Farther from E_{k} the surface $F(\Delta)$ withdraws from $\mathrm{EM}(\Delta)$ with decreasing $|\Delta|$. The load–displacement U is orthogonal to $F(\Delta)$.

(d') For small Δ the stiffness surface $F(\Delta)$ approaches asymptotically a generatrix of the cone of stability $E(P)$ and the load–displacement will approach a generatrix of $\Xi(U)$, the normal cone of $E(P)$ (Proposition 4, Part I).

Example. We consider a semicircular arch, with radius r of the centroid axis, and constant depth d. The arch is loaded along the centroid semicircle by a radial load p constant in each quadrant; $p(s) = p(1 \pm \theta)$, where (+) and (−) signs are attributed to the left and right quadrants, respectively (Fig. 7a and b). To this there corresponds a symmetric load $p_s(s) = p$ and an antimetric load $p_a(s) = \pm\theta p$. We choose the statically determinate state given on Fig. 7a, corresponding to a vertical resultant $P_s = 2rp$ and a horizontal resultant $P_a = \theta 2rp$, respectively, at the centre C of the semicircle and three redundant forces H, Z and X. For the loads P_s, P_a and admissible H, Z and X (with corresponding $|m^i| \leqslant 3$) lower bound approximations of the stiffness D, the stiffness vector $\{\Delta\}$ and the stiffness surface $F(\Delta)$, are determined by Eqs. (34) and (35). The maximum value of D''_σ, corresponding to the actual stiffness D, is attained with the values of H, Z and X, satisfying Eq. (33). These values have been determined for different load-parameters θ and the resulting stiffness surface $F(\Delta)$ is presented in Fig. 7c. The stiffness ellipse $\mathrm{EM}(\Delta)$, the cone $E_k(P)$ of the monolithic core and the cone of stability $E(P)$ of the arch with rigid voussoirs (determined by the linear theory of stability) are

$$\mathrm{EM}: \left(\frac{\Delta_s}{1.1324\sqrt{EA/r}}\right)^2 + \left(\frac{\Delta_a}{0.29638\sqrt{EA/r}}\right)^2 = 1; \quad E_k(P): |P_a| - 0.046505P_s \leqslant 0;$$
$$E(P): |P_a| - 0.28928P_s \leqslant 0 \tag{36}$$

According to (a')–(d') for small θ-values $F(\Delta)$ coincides with $\mathrm{EM}(\Delta)$ within E_k. Outside E_k the curve $F(\Delta)$ gradually withdraws from $\mathrm{EM}(\Delta)$ and finally approaches asymptotically the generatrix of $E(P)$.

5. Stiffness characteristics of a prestressed segmental beam with unbonded tendon

We consider a simply supported centrically prestressed granite beam with one ungrouted tendon and a vertical dry joint at midspan (Fig. 8). The dimensions of the beam are: depth $d = 45$ cm, length $L_0 = 520$ cm, span $L = 510$ cm, width $b = 15$ cm, cross-section $A_c = bd = 677.2$ cm^2, Young's modulus $E_c = 48\,000$ MPa. The tendon: cross-section $A_a = 5.41$ cm^2, Young's modulus $E_a = 202\,000$ MPa, initial prestressing force $F_0 = 474$ kN. F_0 corresponds to a prestressing dislocation

$$[r]^0 = u^0_{xa}(L_0) - u^0_{xc}(L_0) = \frac{F_0 L_0}{E_c A_c}\left(1 + \frac{1}{n\mu}\right); \quad \left(n = \frac{E_a}{E_c};\ \mu = \frac{A_a}{A_c}\right) \tag{37}$$

Two loads $T = P/2$ are applied symmetrically at distance $a = L/3$ from the supports. They induce a moment $M = Pa/2$ at the joint and, together with the prestress F_0, at the lower edge the normal stress

$$\sigma_x(d/2) = -\frac{F_0}{A_c} + 3\frac{Pa}{A_c d} = \frac{F_0}{A_c}(m_0 - 1); \quad m_0 = \frac{3Pa}{F_0 d} \tag{38}$$

where m_0 denotes the nominal relative eccentricity of the compressive force F_0 at the joint. If $m_0 \leqslant 1$, the joint remains closed and $\sigma_x(d/2) < 0$. If $m_0 > 1$, the joint opens, which induces an additional extension $\Delta v_c = \overline{\gamma}(0) = F_a\, d\eta_h(m)/E_c A_c$ of the centroid axis and an increase in the force F_a of the tendon ($F_a > F_0$). Since the dislocation between granite and tendon is fixed to $[r]^0$, we obtain

$$[r] = \frac{F_a}{E_c A_c}\left(L_0\left(1+\frac{1}{n\mu}\right) - d\eta_h(m)\right) = [r]^0; \quad m = \frac{3Pa}{F_a d} > 1 \tag{39}$$

where m is the true relative eccentricity at the joint. Because of the length of the beam segments, the parameter values η_h and α_h comply with Eq. (29). From Eq. (39) we can solve the value $F_a(P)$ iteratively (F_a is contained in the argument m of the very nonlinear function $\eta_h(m)$). Using Eqs. (37) and (39) the prestress can be expressed by F_0 and m

$$F_a = \frac{F_0 L_0(1+n\mu)}{L_0(1+n\mu) - d n\mu\eta_h(m)}; \qquad \frac{m}{m_0} = \frac{L_0(1+n\mu) - d n\mu\eta_h(m)}{L_0(1+n\mu)} \tag{40}$$

The state of stress and strain $\{\sigma,\ u\}$ can be decomposed $\{\sigma,\ u\} = \{\sigma_e, u_e\} + \{\sigma_h, u_h\}$, where $\{\sigma_e, u_e\}$ represents the state of the monolithic beam without tendon loaded by two loads $T = P/2$ with stress distributions

$$\sigma_{xe} = yM(x)/I_c; \quad \sigma_{ye} \approx 0; \quad \tau_{xye} = \frac{3Q}{2A_c}\left(1 - (2y/d)^2\right) \approx 0 \tag{41a, b, c}$$

$\{\sigma_h, u_h\}$ is the state induced by the prestress F_a and the edge effect of the opening joint and where the deformations of the initial state ($F_a = F_0$, $P = 0$) are not included.

The load–displacements U_p are determined according to Section 2, Eqs. (3a) and (3b) using the stresses $\{\sigma_e^a\}$ induced by the loads $P^a = 1/2$

$$U_p = U_{pe} + U_{ph} = \int_0^{L_0} \frac{M^a M\, dx}{E_c I_c} + \frac{a}{2}\int_{A_c} \frac{y\gamma_n}{I_c} dA = \frac{5Pa^3}{12E_c I_c} + \frac{a}{2}\frac{V_h y_h}{I_c} \tag{42a}$$

The first term to the right expresses the load–deflection U_{pe} of the monolithic beam. The second term expresses the edge effect of the opening joint and it can, according to Eq. (10b) and analogously to Eq. (26), be written as

$$U_{ph} = \frac{aV_h y_h}{2I_c} = \frac{a}{2}\omega_h; \quad \omega_h = \frac{F_a d}{E_c A_c k}\alpha_h(m) \tag{42b}$$

where ω_h represents the concentrated rotation at the joint. U_{ph} belongs to the additional deflection $u_{yh}(x)$ of the beam that represents a triangular distribution with an apex at the joint. The load–displacement is thus according to Eqs. (42a) and (42b)

$$U_p = U_{pe} + U_{ph} = \frac{P}{12E_c I_c}\left(5a^3 + \frac{9a^2 d\alpha_h(m)}{m}\right) \tag{43}$$

The extension of the centroid axis v and the mutual rotation ω of the endfaces of the beam are recalling Eqs. (9) and (10a) with $N = 0$ and normal force $N_c = -F_a$ in the granite

$$v = \frac{V_h}{\bar{A}} = \frac{F_a d}{E\bar{A}}\eta_h(m); \quad \omega = \int_0^L \frac{M}{E\bar{I}}dx + \frac{y_h V_h}{\bar{I}} = \frac{Pa^2}{E\bar{I}} + \frac{F_a d\alpha_h(m)}{E\bar{A}k} \tag{44}$$

Formulae (42a), (42b) and (43) presuppose that the material is linearly elastic and the joint interfaces are completely smooth. In reality the roughness of the interfaces increases the deformability and the microcracks in the granite induce nonlinear effects. To these should be added macrocrack phenomena.

The theoretical results were compared with experimental results obtained from a loading test according to Fig. 8. Up to a load $P/2 = 48$ kN cracking did not occur and the greater deformability of the structure tested is clearly perceptible. Instead of vertical cracks a horizontal crack at load $P/2 = 48$ kN discontinuously increased the displacements. This was caused by the transverse tensile stress σ_y at the joint with the greatest value

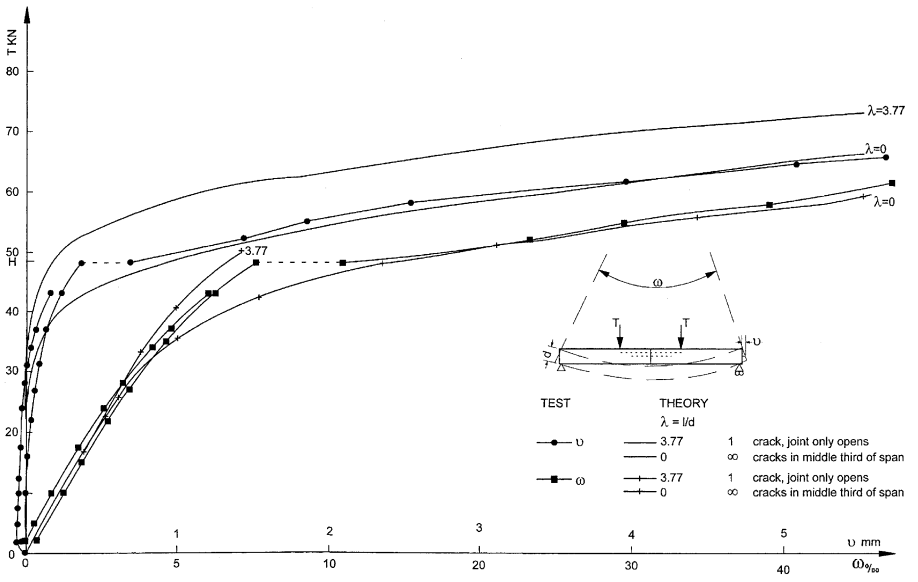

Fig. 9. Prestressed granite beam; elongation v and rotation ω.

$$\max \sigma_y \cong \frac{F_a}{A_c} \frac{(|m|-1)}{(3-|m|)} \tag{45}$$

which exceeded the maximum longitudinal tensile stress $\sigma_x(d/2)$ (Eq. (38)) of the undisturbed part of the segment. The maximum σ_y at the joint occurs close to the border of the contact region, where $\sigma_x, \gamma_n \to 0$. Because the compressive stress distribution $\sigma_x(y)$ approximately approaches the triangular distribution corresponding to crack distance $\lambda = 0$, the horizontal crack reduces the effective depth of the beam from d to $d_0 = (3-|m|)d/2$. This implies that in the middle third of the span the effect of the longitudinal crack on the displacements corresponds to deformation parameters (Eq. (26)) at $\lambda = 0$ (Parland, 1995)

$$\delta_{0h} \cong \frac{(|m|-1)^3}{3(3-|m|)} \frac{a}{d}; \quad \eta_{0h} \cong \frac{(|m|-1)^2}{(3-|m|)} \frac{a}{d}; \quad \alpha_{0h} \cong \frac{(4-|m|)(|m|-1)}{3(3-|m|)} \frac{a}{d} \tag{46}$$

Using these values, upper bounds for u_p, v_h and ω_h for loads above the cracking load $P/2 = 48$ kN are calculated. The results are shown in Figs. 8 and 9.

6. Indentation of an elastic strip on a rigid foundation by a rigid punch

Let the height of the strip be d and its thickness t, let the profile of the punch be $h(x) = U_2|x|^n$ and its width be d_p. The contact problem of the strip can be treated in two ways (Gladwell, 1980, Parland and Miettinen, 1985):

(a) The nonlinear problem: the prescribed vertical load $P_1^* = \int_{\Gamma_c} p_y \, dx$ acts on an inextensible cover of the strip with unchanged profile $h(x) = U_2^*|x|^n$, that defines the initial vertical gap $[r]_y$. The contact area Γ_c increases monotonously with the load P_1^*. The displacements $\mathbf{u}_c(x)$ of the cover on Γ_c are determined by the prescribed U_2^* and the vertical translation U_1^0 of the punch. We have thus the conditions

$$u_{cy}(x) = U_1^0 - U_2^*|x|^n; \qquad u_{cx}(x) = 0 \tag{47a}$$

$$\int_{\Gamma_c} p_y \,\mathrm{d}x = P_1^* \tag{47b}$$

(b) The semilinear problem: by releasing U_2 we get according to Part I, Appendix A the complementary conditions

$$u_{cy}(x) = U_1^0 - U_2^0|x|^n; \qquad u_{cx}(x) = 0 \tag{48a}$$

$$\int_{\Gamma_c} p_y \,\mathrm{d}x = P_1^*; \qquad \int_{\Gamma_c} p_y |x|^n \,\mathrm{d}x = P_2^*; \qquad \int_{\Gamma_c} p_x \,\mathrm{d}x = 0 \tag{48b}$$

The load is defined by the prescribed vertical resultant P_1^* and the prescribed P_2^* that represents the nth moment of the vectors $p_y \,\mathrm{d}x$. The initial gap is zero ($[r] = 0$) and the profile of the punch deforms continuously with $h(x) = U_2^0|x|^n$ and U_1^0 and U_2^0 depend linearly on P_1^* and P_2^*. When $P_1^* > 0$ the contact area decreases discontinuously from d_p to the fixed value $2a$. In this case the multiplicity rule applies.

The difference between nonlinear and semilinear loading manifests itself by the zero point x_n of $u_y(x, 0)$ that expresses a nominal extent of the penetration (Fig. 10) defined by

$$\xi_n = x_n/d = \sqrt[n]{U_1/U_2}/\mathrm{d} \tag{49}$$

At nonlinear loading U_2^* is fixed whereas U_1 increases with P_1^*. Therefore the penetration is represented by parallel curves (Fig. 10a). At semilinear loading the ratio U_1/U_2 is independent of the load intensity and ξ_n attains a fixed value (Fig. 10b) at increasing load P_1^*.

In the semilinear problem with load intensity P_1^*, P_2^* the external work of the load is

$$\int_{\Gamma_c} p_y u_y \,\mathrm{d}x = U_1^0 \int_{\Gamma_c} p_y \,\mathrm{d}x - U_2^0 \int_{\Gamma_c} |x|^n p_y \,\mathrm{d}x = P_1^* U_1^0 - P_2^* U_2^0 = P_1^* U_P \tag{50a}$$

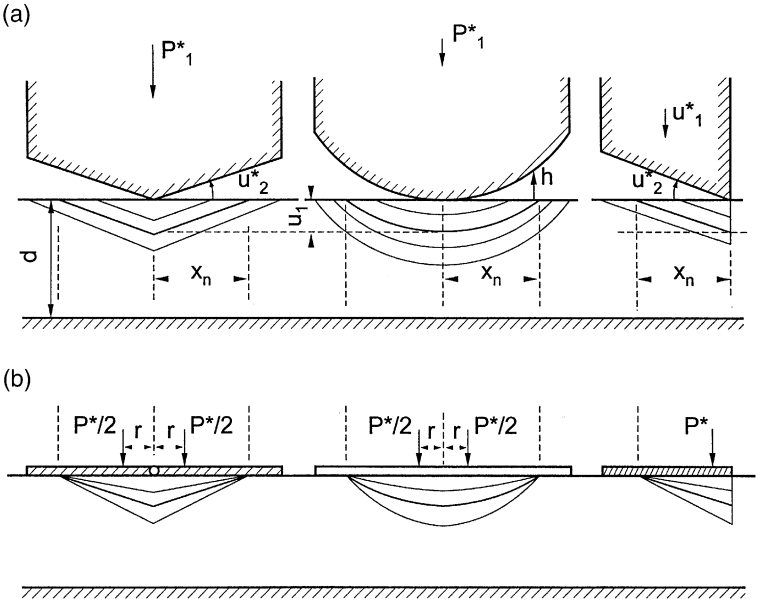

Fig. 10. Indentation of elastic strip. (a) Nonlinear loading. (b) Semilinear loading.

where $U_P = U_1^0 - (P_1^*/P_2^*)U_2^0$. The external work equals the internal work $2W + \langle p, \gamma \rangle$, where on the upper ($y = 0$) edge $\langle p, \gamma \rangle_{\Gamma_c} = t \int_{\Gamma_c} |\sigma||\gamma_t|(\tan\varphi - \tan\beta)\,dx$ and on the lower ($y = d$) edge we presuppose $\langle p, \gamma \rangle = 0$. Using the notations $\kappa = a/d$ and $md^n P_1^* = P_2^*$ (Fig. 11) and

$$P_1^* U_P = 2W + \langle p, \gamma \rangle_{\partial Y} \tag{50b}$$

we can express U_1^0 and U_2^0 as functions of P_1^*, m and κ, which in turn are functions of φ and β. If the multiplicity rule applies we get

$$U_1^0(\kappa) = \frac{P_1^*}{Et}\eta(m,\kappa); \qquad \mathrm{U}_2^0(\kappa) = \frac{P_1^*}{Etd^n}\theta(m,\kappa); \qquad U_P(\kappa) = \frac{P_1^*}{Et}\delta(m,\kappa) \tag{51a}$$

In the limit state of free contact $\eta(m,\kappa)$, $\theta(m,\kappa)$ and $\delta(m,\kappa)$ attain at $\kappa_0 = a_0/d$ extreme values $\eta(m)$, $\theta(m)$ and $\delta(m)$ with displacements

$$U_1^0 = \frac{P_1^*\eta(m)}{Et}; \qquad U_2^0 = \frac{P_1^*\theta(m)}{Etd^n}; \qquad U_P = \frac{P_1^*\delta(m)}{Et} \tag{51b}$$

where U_P is the displacement of $P_1^*/2$ at the distance $r = m^{1/n}d$ from the origin. The parameters η, θ and δ satisfy

$$\delta(m) = \eta(m) - m\theta(m) \tag{51c}$$

With load intensity $|P_1^*|$ the corresponding stiffness is

$$D = \frac{|P_1^*|}{U_P} = \frac{Et}{\delta(m)} \tag{52}$$

If the friction is nondissipative, then there applies

$$W_\sigma = \frac{1}{2}P_1^* U_P = \frac{(P_1^*)^2}{2Et}\delta(m); \qquad \theta = -\frac{1}{2}\frac{\partial\delta}{\partial m}; \qquad \eta = -\frac{m^3}{2}\frac{\partial}{\partial m}\left(\frac{\delta}{m^2}\right) \tag{53a, b, c}$$

In Appendix A are given the calculations for frictionless indentation by a wedgeshaped punch ($n = 1$), a parabolic punch ($n = 2$) and an eccentrically loaded rectangular punch ($n = 0$). The results are shown in Figs. 11–13.

In the nonlinear case, with U_2^* fixed and $\varphi = 0$, the initial gap is $[r]_y = U_2^*|x|^n$. With $\gamma_n = -[r]_y$ and $\langle p, \gamma_n \rangle = P_2^0 U_2^*$ the work of the load P_1^* is

$$P_1^* U_1^0 = 2W + P_2^0 U_2^*, \quad \text{where } P_2^0 = t\int_{-a}^{a} |\sigma||x|^n\,dx \tag{54}$$

We have in this case advancing contact, where $P_1^*\theta = Etd^n U_2^*$ and the contact area Γ_c increases, with the load P_1^*, gradually from zero to $2a$. Using the expressions (51b) we obtain at given P_1^* and U_2^*

$$\overline{P}_1 = \frac{P_1^*}{Etd^n U_2^*} = \frac{1}{\theta}; \qquad \overline{U}_P = \frac{U_P}{d^n U_2^*} = \frac{\delta(\theta)}{\theta}; \qquad \overline{U}_1 = \frac{U_1^0}{d^n U_2^*} = \frac{\eta(\theta)}{\theta} \tag{55}$$

where $\overline{P}_1$ represents the dimensionless load and $\overline{U}_1^0$ the dimensionless translation of the rigid punch, being proportional to the nth power of the nominal penetration width (Eq. (49)). In this case upper bound solutions $\{u', \gamma'\}$ and lower bound solutions $\{u'', \sigma''\}$ with $\theta'(m') = \theta''(m'') = \theta(m)$ correspond to different values of m', m'' and m.

The stiffnesses $D_p = P_1^*/U_p$ and $D_1 = P_1^*/U_1^0$ are expressed by the dimensionless stiffnesses as functions of θ

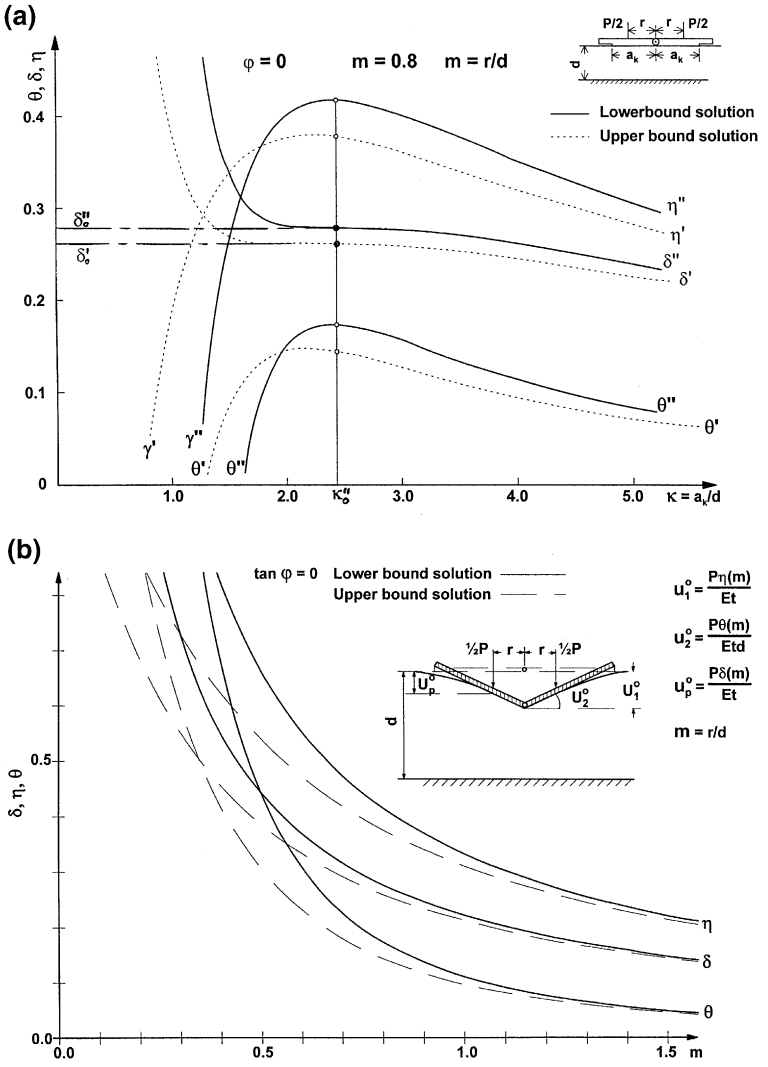

Fig. 11. Semilinear indentation of strip by a wedge. (a) Dependence of stiffness parameters on a_k/d; they attain stationary values in the limit state. (b) Stiffness parameters versus load distance $m = r/d$.

$$\overline{D}_p = \frac{\overline{P}_1}{\overline{U}_p} = \frac{1}{\delta(\theta)}; \qquad \overline{D}_1 = \frac{\overline{P}_1}{\overline{U}_1} = \frac{1}{\eta(\theta)} \tag{56}$$

The corresponding load–displacement and stiffness-curves for $n = 1$ are given in Fig. 14.

If the friction is purely dissipative ($\beta = 0$, $\varphi = \rho$), the stiffness characteristics depend on the dissipative work. In the semilinear case this can be written as

$$\langle p, \gamma \rangle = t \int_{\Gamma_c} |\sigma||\gamma_t| \tan\varphi \, dx \tag{57a}$$

with the bounds (Part I, Eq. (77a)) at the same external load P_1^*

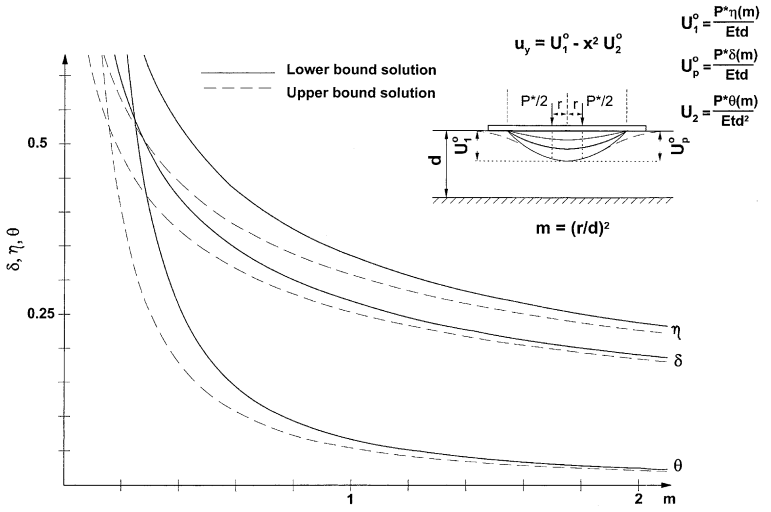

Fig. 12. Parabolic punch; semilinear indentation, $\tan\varphi = 0$.

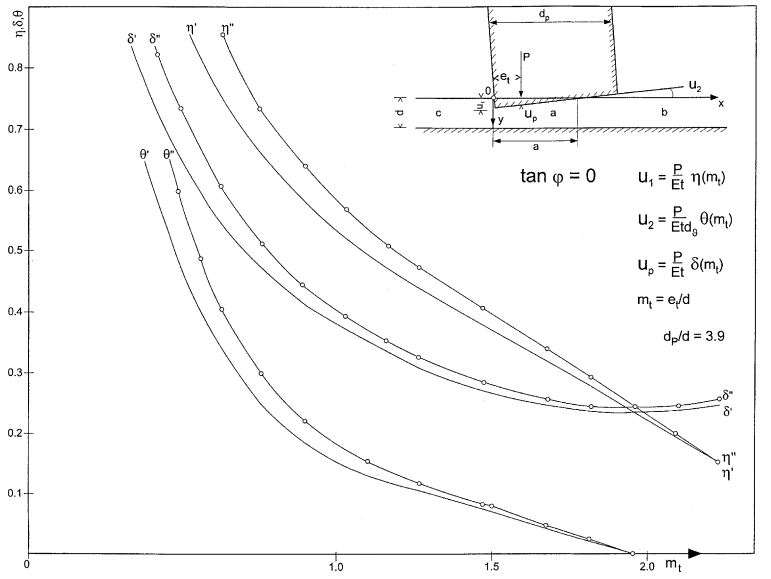

Fig. 13. Indentation of a strip by a rectangular punch; (- - -) upper bound solution, $\tan\varphi = 0$, (- - -○- - -) lower bound solution, $\tan\varphi = 0$.

$$\langle p^{\mathrm{f}}, \gamma^{\mathrm{f}} \rangle_{\varphi,0} \cong \langle p, \gamma \rangle \leqslant \langle p^{\mathrm{b}}, \gamma^{\mathrm{b}} \rangle_{\varphi,0} \tag{57b}$$

where $\{p^{\mathrm{f}}, \gamma^{\mathrm{f}}\}$ and $\{p^{\mathrm{b}}, \gamma^{\mathrm{b}}\}$ correspond to the solutions of the nondissipative problem with $\beta^{\mathrm{f}} = \varphi$ and $\beta^{\mathrm{b}} = 0$, respectively. The corresponding work expressions are

$$\langle p^{\mathrm{f}}, \gamma^{\mathrm{f}} \rangle_{\varphi,0} = t \int_{-a_0}^{a_0} \left|\sigma^{\mathrm{f}}\right| \left|\gamma_{\mathrm{t}}^{\mathrm{f}}\right| \tan\varphi \, \mathrm{d}x; \qquad \langle p^{\mathrm{b}}, \gamma^{\mathrm{b}} \rangle_{\varphi,0} = t \int_{-a_0}^{a_0} \left|\sigma^{\mathrm{b}}\right| \left|\gamma_{\mathrm{t}}^{\mathrm{b}}\right| \tan\varphi \, \mathrm{d}x \tag{57c}$$

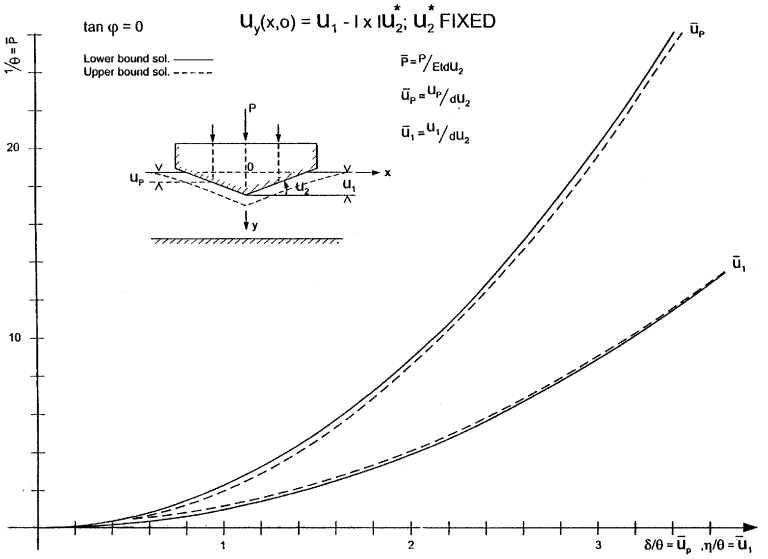

Fig. 14. Nonlinear indentation of strip. Increasing contact. Relative load $\overline{P}$ of wedge versus relative load–displacements $\overline{U}_1$ and $\overline{U}_P$.

The integrals in Eqs. (57a) and (57c) are confined to the slip-region $\Gamma_s < 2a_0$. Choosing as load intensity P_1^*, the work equation for purely dissipative friction ($\varphi \neq 0$; $\beta = 0$) is

$$P_1^* U_P(\varphi, 0) = 2W + t \int_{\Gamma_c} |\sigma||\gamma_t| \tan\varphi \, dx \tag{58}$$

Recalling that $U_P = U_1 - md^n U_2$, and Eqs. (78c), (79a) and (80b) of Part I, and using the notation $c = \langle p_1^f, \gamma^f \rangle_{\varphi,0} / (P_1^*)^2$, we obtain the estimates

$$\sup \delta(m, \varphi, 0) \leqslant \left\{ \begin{array}{c} \delta_i(m, \varphi, 0) = \frac{\delta(m,0,0)}{2} \left(1 + \left(1 - \frac{4Etc}{\delta(m,0,0)} \right)^{1/2} \right) \\ \delta_{ii}(m, \varphi, 0) = \frac{\delta(m,0,\varphi)}{2} \left(1 + \frac{4Etc}{\delta(m,0,\varphi)} + \left(1 + \frac{4Etc}{\delta(m,0,\varphi)} \right)^{1/2} \right) \end{array} \right\} \tag{59}$$

$$\inf \delta(m, \varphi, 0) \geqslant \delta_s(m, \varphi, 0) = \delta(m, 0, \varphi) + Etc$$

From Eq. (59) estimates of $U_p = P_1^* \delta(m, \varphi, 0)/Et$ and of the stiffness $D(m, \varphi, 0) = P_1^*/U_p = Et/\delta(m, \varphi, 0)$ are obtained (Fig. 15a).

In the nonlinear case the gap deformation, where $p_y > 0$, is as before $\gamma_n = -h$. The work equation at the friction (φ, 0) is therefore with $\mathbf{p}_{\mu\nu} = \tau\mathbf{i} + |\sigma|\mathbf{j}$; $\boldsymbol{\gamma}_{\nu\mu} = \gamma_x \mathbf{i} - h\mathbf{j}$

$$P_1^* U_1 = 2W + t\langle \tau, \gamma_x \rangle - t\langle |\sigma|, \gamma_y \rangle = 2W + t \int_{-a}^{+a} \tau\gamma_x \, dx + t \int_{-a}^{+a} |\sigma| h(x) \, dx \tag{60}$$

The work $\int \tau\gamma_x \, dx$ is positive if no reversals of slip occur. Because $h(x) = |x|^n U_2^*$ and $P_2^0 = t \int_{-a}^{a} |\sigma||x|^n \, dx = md^n P_1^*$, we can write, according to Eq. (58),

$$P_1^* U_1 = 2W + t \int \tau\gamma_x \, dx + P_2^0 U_2^* = P_1^* U_P(\varphi, 0) + md^n P_1^* U_2^* \tag{61}$$

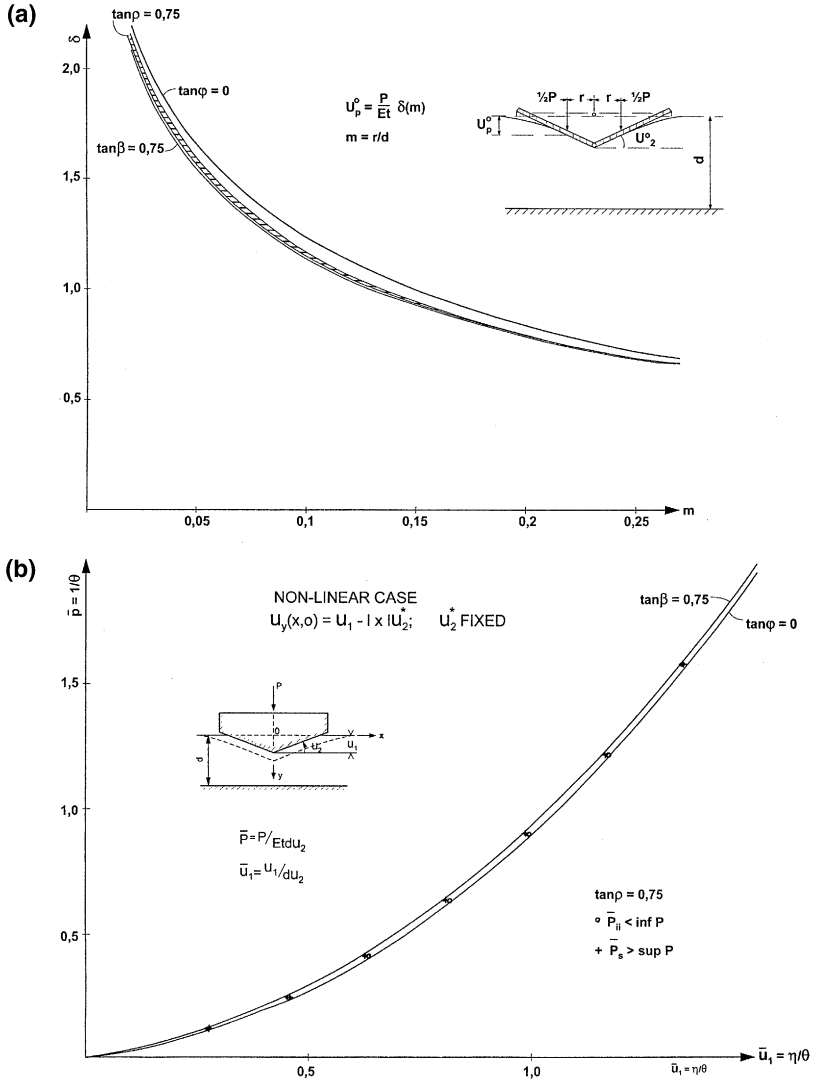

Fig. 15. Indentation of a strip by a wedge, $\tan\varphi = 0.75$. (a) Semilinear case, shaded area corresponding to $\tan\rho = 0.75$ (b) nonlinear case.

where $P_1^* U_P$ corresponds to the semilinear problem. Eq. (61) can according to Eqs. (51a)–(51c) with $U_2^*/P_1^* = \theta^*$ be written as

$$P_1^* U_1 = \frac{(P_1^*)^2}{Et}\eta(\theta^*, \varphi, 0) = \frac{(P_1^*)^2}{Et}(\delta(\theta^*, \varphi, 0) + m\theta^*) \tag{62}$$

From this we get for given θ^* the upper bound estimates

$$\sup \eta(\theta^*, \varphi, 0) < \begin{cases} \delta_i(\theta^*, \varphi, 0) + \sup\limits_{\beta}(m(\beta)\theta^*) \\ \delta_{ii}(\theta^*, \varphi, 0) + \sup\limits_{\beta}(m(\beta)\theta^*) \end{cases} \tag{63}$$

Analogously a lower bound for $P_1^* U_1$ at given U_2^* is obtained

$$\inf \eta(\theta^*) \geqslant \delta_s(\theta^*, \varphi, 0) + \inf_{\beta}(m(\beta)\theta^*) \tag{64}$$

where β is restricted to the interval $[0, \varphi]$. From Eqs. (63) and (64) corresponding estimates of the stiffness $D_1 = P_1^*/U_1 = Et/\eta(\theta)$ are determined (Fig. 14b).

7. Summary and conclusions

The theoretical results of Part I are applied to structures with contact problems. Particular attention is paid to the inter-relations of the following characteristics:

1. The cone of the monolithic core $E_k(P, \rho, \beta)$, where the principle of superposition remains valid.
2. The stiffness ellipsoid $\mathrm{EM}(P)$ of the monolithic structure.
3. The stiffness $D(P, \rho, \beta)$ and the stiffness surface $F(\Delta, \rho, \beta)$, where $\Delta = \sqrt{D(P, \rho, \beta)}P/|P|$ denotes the stiffness vector.
4. The cone of stability $E(P, \rho, \beta)$ of the structure.

The effect of dry joints and cracks on a generalized displacement U^i can be extracted by decomposing the state of stress and displacement $\{\sigma,\ u\}$, at given loads, into a state $\{\sigma_e,\ u_e\}$ of the elastic monolithic structure and a state $\{\sigma_h,\ u_h\}$ induced by the discontinuities at the joints Γ_r. Using the stressfield $\{\sigma_e^i\}$ induced by load $P^i = 1$ acting at region Γ_j, U^i is then expressed by

$$U^i = U_e^i + U_h^i; \quad U_h^i = \sum_r \int_{\Gamma_r} \mathbf{p}_e^i \cdot \boldsymbol{\gamma}\, \mathrm{d}\Gamma = \sum_r w_r^i$$

where U_e^i and U_h^i are the generalized displacements of the monolithic structure and a quasi rigid structure, respectively. The w_r^i represent generalized discontinuities, including translations and rotations at joint r. In this way it is possible to decompose the nonmonolithic structure into a monolithic elastic structure and a quasi rigid structure that deforms with partial interpenetration at the joints. The above transformation of displacement discontinuities implies actually an extension of Reissner's condensation of the laws governing the displacement field of plates.

The following structures have been analysed using the principle of complementarity and the extremum principles of stiffness and extent of contact:

(a) A rectangular panel eccentrically pressed against rigid support.
(b) Loading of a semicircular elastic voussoir arch.
(c) Bending of a prestressed segmental beam.
(d) Indentation of an elastic strip by a rigid punch.

The decomposition into a monolithic part and a quasi rigid part is most obvious in case (b) (Fig. 6 Voussoir arch), but it is clearly perceptible also in case (c) (Fig. 8).

Concerning the friction we can distinguish between two cases:

(i) Frictional contact sliding does not occur ($0 \leqslant |\tau| < |\sigma| \tan \varphi$; includes frictionless contact).
(ii) Frictional contact sliding does occur ($0 < |\tau| \leqslant |\sigma| \tan \varphi$).

In case (i) the solution is independent of the path of loading and unique, if during loading the condition $|\tau| < |\sigma| \tan \varphi$ holds. Nonlinear contact problems with initial gaps at the joints ($h > 0$) and prestress ($\sigma_0 < 0$) can be transformed into semilinear problems ($h = 0$, $\sigma_0 = 0$) by change of structure and loading. These results have been applied to a prestressed segmental beam and to indentation problems. For the latter case upper and lower bounds of stiffness and corresponding generalized displacements have been obtained by elementary means (Fig. 12). From these results the displacement parameters of the nonlinear cases with rigid stamps have been determined (Fig. 14).

In case (ii) with frictional contact sliding the solution depends on the loading path and is generally not unique also at proportional loading. In this case with semilinear loading (i.e. $\sigma_0 = [r] = 0$) the stiffness proper $D(P, \varphi, 0)$ in contrast to other characteristics approaches $D(P, 0, \varphi)$ from below, the closer the more continuous the contact is. In many cases the stiffness corresponding to nondissipative friction provides sufficiently close bounds for $D(\varphi, 0)$ with $D(0, 0) < D(\varphi, 0) < D(0, \varphi)$. Still closer bounds can be established for the infima and suprema of the stiffness $D(\varphi, 0)$ using the contact sliding components $\boldsymbol{\gamma}_t$ of the nondissipative solution.

The examples of Part II indicate thus that the complications caused by the indeterminateness connected with dissipative friction can at proportional loading be effectively reduced by the use of nondissipative friction with conical restraints of the deformations $\boldsymbol{\gamma}$ at the joints.

Acknowledgements

This work has been carried out at the laboratory of Structural Mechanics, Department of Civil Engineering, Tampere University of Technology and has been supported by the Svenska tekniska vetenskapsakademien i Finland.

Appendix A. Indentation without friction. Semilinear loading

To begin with we assume the interfaces at $y = 0$ and d to be detachable ($\gamma \geqslant 0$) and smooth ($\varphi, \beta = 0$). For $n = 1$, the semilinear case materializes if we replace the rigid wedge by two rigid plates connected by a hinge and loaded by two symmetrical loads $P_1^*/2$ at distances r from the hinge. The symmetry leads to the equilibrium conditions at $x = 0$ (Part I, Appendix A)

$$Q_y(0) = \int_0^a p_y \,\mathrm{d}x - P_1^*/2 = 0; \quad M(0) = rP_1^*/2 - \int_0^a |x| p_y \,\mathrm{d}x = 0 \tag{A.1}$$

A lower bound $D_\sigma''(0,0)$ of the stiffness is obtained assuming a vertical uniaxial compression field $\{\sigma_y''(x,y) = -p_y(x)/t, \sigma_x'' = \tau_{xy}' = 0\}$, with corresponding stress energy $W_\sigma'' = td \int (\sigma_y'')^2 \,\mathrm{d}x/2E$. According to the principle of the maximum stiffness, an optimal W_σ'' where $t\sigma_y = -p_y$ is subjected to the constraints (A.1), at given a, corresponds to

$$\min_\sigma W_\sigma''(0,0) = \frac{\mathrm{d}}{Eat}\left((P_1^*)^2 - 3P_1^*P_2^*/a + 3(P_2^*/a)^2\right) \tag{A.2}$$

The limit state of free contact is according to Proposition 5, Part I attained at the value $a_0 = 3P_2^*/P_1^*$, where $\min(W_\sigma'')$ attains a supremum and the displacements U_1 and U_2 attain extrema. Hence there applies according to Castiglianos's rule

$$\sup_a \left(\min_\sigma W_\sigma''(0,0)\right) = \frac{\mathrm{d}(P_1^*)^3}{3EtP_2^*}; \quad U_1'' = \frac{\mathrm{d}(P_1^*)^2}{3EtP_2^*}; \quad U_2'' = \frac{\mathrm{d}(P_1^*)^3}{9Et(P_2^*)^2}; \quad U_P'' = \frac{2\mathrm{d}(P_1^*)^2}{9EtP_2^*} \tag{A.3}$$

With $m = P_2^*/(\mathrm{d}P_1^*)$ and $\kappa_0'' = d_0''/d = 3m$, the parameters η, θ and δ of Eqs. (51b) and (51c) attain the values

$$\delta''(m) = \frac{2}{9m}; \quad \eta''(m) = \frac{1}{3m}; \quad \theta''(m) = \frac{1}{9m^2} \tag{A.4}$$

An upper bound solution is obtained using the continuous displacement fields:

Region I: $|x| \leqslant a$; $0 \leqslant y \leqslant d$

$$u_y = (U_1 - U_2|x|)(1 - y/d); \qquad u_x = v(U_1 x - U_2 x^2/2)/d \tag{A.5}$$

with $\varepsilon_y = -(U_1 - U_2|x|)/d$; $\varepsilon_x = -v\varepsilon_y$; $\gamma_{xy} = -(1 - y/d)U_2 \mathrm{sign}(x)$

Region II: $|x| > a$ and $|x'| = a + a_1 - |x|$; $|x'| \leqslant a_1$

$$u_y' = (U_1' - aU_2')(1 - y/d)x'/a; \qquad u_x' = v(U_1' - aU_2')x'/(2a_1 d) + C \tag{A.6}$$

with $\varepsilon_y' = (U_1' - aU_2')x'/(a_1 d)$; $\varepsilon_x' = -v\varepsilon_y'$; $\gamma_{xy}' = (U_1' - aU_2')x'/(a_1 d)$

Region III: If $|x| > a + a_1$ then $u_x = u_y \equiv 0$.

The potential energy of the system is

$$\pi = \frac{Et}{2} \int_0^d \int_{-a-a_1}^{a+a_1} \left(\varepsilon_y^2 + \frac{\gamma_{xy}^2}{2(1+v)} \right) \mathrm{d}x\,\mathrm{d}y - P_1^* U_1 + P_2^* U_2 \tag{A.7}$$

By inserting the formulas for ε_y and γ_{xy} from Eqs. (A.5) and (A.6) and denoting $a'/d = \kappa'$, $a_1'/d = \kappa_1'$ and $c_1 = \kappa' + \kappa_1'/3$, $c_2 = \kappa'(\kappa' + 2\kappa_1'/3)$, $c_3 = \kappa'(\kappa' + \kappa_1')^2/3$ the potential energy gets the form

$$\pi = Et(c_1(U_1')^2 - 2c_2 U_1' U_2' + c_3(U_2')^2) - P_1^* U_1' + P_2^* U_2' \tag{A.8}$$

The minimum condition of π with respect to U_1', U_2' and κ_1' gives $\kappa_1' = (2 + 2v)^{-1/2}$ and according to Eq. (51a)

$$\delta'(m, \kappa') = \frac{c_1 m^2 - 2c_2 m + c_3}{2(c_1 c_2 - (c_2)^2)}; \quad \eta'(m, \kappa') = \frac{c_3 - c_2 m}{2(c_1 c_3 - (c_2)^2)}; \quad \theta'(m, \kappa') = \frac{c_2 - c_1 m}{2(c_1 c_3 - c_2)} \tag{A.9}$$

These parameters depend on $\kappa' = a'/d$ and because κ_0' differs only little from the value κ_0'' of the AE state we can choose $\kappa_0' = \kappa_0'' = 3m$. The corresponding values $\delta''(m)$, $\eta''(m)$, $\theta''(m)$ and $\delta'(m)$, $\eta'(m)$, $\theta'(m)$ are shown in Fig. 11b. Because of the extremum principles of stiffness, there holds

$$\delta'(m) \leqslant \delta(m) \leqslant \delta''(m) \tag{A.10}$$

The approximate solutions for semilinear problem of a punch with a parabolic profile ($n = 2$) $h(x) = U_2^* x^2$ (Fig. 12) can be solved analogously. In the lower bound solution with $P_2^* = md^2 P_1^*$ the contact area is determined by the limit value $\kappa_0'' = (5m)^{-1/2}$ and the stiffness parameters are

$$\delta''(m) = 0.6(5m)^{-1/2}; \quad \eta''(m) = 0.75(5m)^{-1/2}; \quad \theta''(m) = 0.75(5m)^{-3/2} \tag{A.11}$$

An upper bound solution is obtained by replacing $|x|$ by x^2 in Eqs. (A.1) and (A.5). The stiffness parameters are obtained from Eq. (A.9) by using

$$c_1 = \frac{3(\kappa' + \kappa_1') + \kappa'^3}{3}; \quad c_2 = \frac{\kappa'^2(\kappa' + \kappa_1') + \kappa_1'^3}{3}; \quad c_3 = \frac{\kappa'^3(\kappa'(3\kappa' + 5\kappa_1') + 5\kappa_1'(\kappa' + 4\kappa_1'/3))}{15} \tag{A.12}$$

where again $\kappa_0' = \kappa_0'' = (5m)^{1/2}$ provides a good approximation.

Smooth indentation ($\tan\varphi = 0$) by a rectangular punch corresponds to $n = 0$. The strip is resting on a rigid foundation without friction but with adherence, $u_y(x, d) = 0$. The width of the punch is d_p and the load

is applied eccentrically at $x_p = e_t = m_t d$ (Fig. 13). An upper bound solution with corresponding lower bounds for parameters $\eta'(m_t)$, $\theta'(m_t)$ and $\delta'(m_t)$ are determined by FEM using a continuous displacement field in the strip.

A lower bound solution for the inclined punch is obtained by using three different stress-functions F^a in the contact region a, F^b in region b to the right and F^c in region c to the left of a

$$\begin{aligned} F^a &= g_a(\zeta)(1-\cos\pi\upsilon) + f(\zeta); \quad 0 \leqslant \upsilon \leqslant \upsilon_0 \\ F^b &= g_b(\zeta)(1-\cos\pi\upsilon); \quad \upsilon_0 \leqslant \upsilon < \infty \\ F^c &= g_c(\zeta)(1-\cos\pi\upsilon); \quad -\infty < \upsilon \leqslant 0 \end{aligned} \tag{A.13}$$

where $\zeta = x/d$, $\upsilon = y/d = 2y/\lambda d_p$. The stresses corresponding to functions F^i are

$$\sigma_x^i = g_i\pi^2\cos\pi\upsilon; \quad \sigma_y^i = g_i''(1-\cos\pi\upsilon)/d^2 + \delta_{ia}f''/d^2; \quad \tau_{xy}^i = -(g_i'\pi\sin\pi\upsilon)/d^2 \tag{A.14}$$

where i = a, b, c, and the commas denote differentiation with respect to ζ.

Because $\tau_{xy} = 0$ on the upper and lower edges of the strip and at $|x| = \infty$ the stress energy is

$$W = t/(2E)\int\int(\sigma_x + \sigma_y)^2\,\mathrm{d}x\,\mathrm{d}y \tag{A.15}$$

Using Kantorovich's method, a solution is obtained by minimizing W with the conditions on the upper edge, Eq. (A.16), and the continuity and limit state conditions, Eq. (A.17), at $x = 0$ and $x = a$

$$-t\int_0^a \sigma_y^a(x,0)\,\mathrm{d}y = P; \quad -t\int_0^a y\sigma_y^a(x,0)\,\mathrm{d}y = Pe_t; \quad \sigma_y^b(x,0) = \sigma_y^c(x,0) = 0 \tag{A.16}$$

$$\sigma_x^a(0,y) = \sigma_x^c(0,y); \quad \sigma_x^a(a,y) = \sigma_x^b(a,y); \quad \tau_{xy}^a(0,y) = \tau_{xy}^c(0,y); \quad \tau_{xy}^a(a,y) = \tau_{xy}^b(a,y) \tag{A.17}$$

The minimum condition of W provides expressions for g_a, g_b, g_c and f''

$$\begin{aligned} g_a &= A_a\cosh\pi\zeta + B_a\pi\zeta\cosh\pi\zeta + C_a\sinh\pi\zeta + D_a\pi\zeta\sinh\pi\zeta \\ g_b &= \mathrm{e}^{-\alpha\zeta}(A_b\cos\beta\zeta + B_b\sin\beta\zeta); \quad \alpha = 0.6748\pi \\ g_c &= \mathrm{e}^{\alpha\zeta}(A_c\cos\beta\zeta + B_c\sin\beta\zeta); \quad \beta = 0.3493\pi \\ f'' &= -g_a'' + Ed(U_1 - \mathrm{d}\zeta U_2) \end{aligned} \tag{A.18}$$

From Eqs. (A.16) and (A.17) the 10 unknown constants $A_a, B_a, \ldots, U_1, U_2$ are determined as functions of P and $m_t = e_t/d$. We express the generalized displacements by

$$U_1 = \frac{P}{Et}\eta(m_t); \quad U_2 = \frac{P}{Etd}\theta(m_t); \quad U_P = u_y(e_t,0) = \frac{P}{Et}\delta(m_t) \tag{A.19}$$

where $u_x(x,0) = U_1 - xU_2$. These U_1, U_2, U_P correspond to contact length a, that is smaller than the width d_p of the punch. Let the value m_{td} correspond to $a = d_p$ with $\sigma_y^a(d_p,0) = 0$. We obtain the eccentricities for $m_t > m_{td}$ using the superposition Lemma B.1 (Appendix B) for unchanged contact regions by applying the load $P^1 = (1-\kappa)P$ at $x_1 = e_{td} = m_{td}d$, and $P^2 = \kappa P$ at $x_2 = d_p - e_{td}$. The resulting eccentricities are therefore, with $d_p = 2d/\lambda$ and $0 \leqslant \kappa \leqslant 1$

$$e_t = (1-\kappa)e_{td} + \kappa(d - e_{td}) = e_{td} + \kappa(d - 2e_{td}); \quad m_t = m_{td} + \kappa(2/\lambda - 2m_{td}) \tag{A.20}$$

P^1 induces $u_y^1(0,0) = (1-\kappa)U_1^1$ and P^2 induces $u_y^2(0,0) = \kappa(U_1^2 - U_2^2 d) = \kappa(U_1^2 - 2d_a U_2^2/\lambda)$, where U_1^1 and U_2^1 correspond to P^1 at $x = e_{td}$ and U_1^2 and U_2^2 correspond to P^2 at $x = d_p - e_{td}$. But because of the symmetric position of P^1 and P^2 with respect to the midpoint $x = d_p/2$, there holds: $U_1^2 = U_1^1$; $U_2^2 = U_2^1$. Applying the superposition rule we obtain finally

$$u(x,0) = U_1 - xU_2$$
$$U_1 = (1-\kappa)U_1^1 + \kappa(U_1^1 - 2d_a U_2^1/\lambda) = U_1^1 - 2d\kappa U_2^1/\lambda \tag{A.21}$$
$$U_2 = (1-\kappa)U_2^2 - \kappa U_2^2 = (1-2\kappa)U_2^2$$

Recalling Eq. (A.19) we obtain

$$\eta(m) = \eta(m_{td}) - 2\kappa\theta(m_{td})/\lambda$$
$$\theta(m) = (1-2\kappa)\theta(m_{td}) \tag{A.22}$$
$$\delta(m) = \beta(m_{td}) - m_{td}\theta(m_{td})$$

Thus we can determine the stiffness parameters for all eccentricities e_t in the interval $0 < e_t < d_p$ (Fig. 13).

In frictionless case applying the superposition lemma (Appendix B) the deductions for the rectangular punch can be used to determine the stiffness characteristics for an eccentrically loaded rigid punch on the elastic strip. Let a centrical load P_c on the punch with symmetrical profile $y_0 = U_{2c}|d_p/2 - x|^n$ and width d_p induce a state $\{u_c\}$ of complete contact with contact length $a = d_p$. The superposition of $\{u_c\}$ on any solution of limit state $\{u_r\}$ with the same contact length $a_r = d_p$ of a rectangular punch loaded by an eccentrical load $P_r = \kappa P_c$ provides then a solution $\{u\}$ for an eccentrically loaded punch with an arbitrary symmetric profile

$$\{u\} = \{u_c\} + \{u_r\}; \quad u_{cy} = U_{1c} - U_{2c}|d_p/2 - x|^n; \quad u_{ry} = U_{1r} - xU_{2r} \tag{A.23}$$

where

$$U_{1c} = \frac{P_c}{Et}\eta_c; \quad U_{1r} = \frac{\kappa P_c}{Et}\eta_r(m_{td})$$
$$U_{2c} = \frac{P_c}{Etd}\theta_c \text{ fixed}; \quad U_{2r} = \frac{\kappa P_c}{Etd^n}\theta_r(m_{td}) \tag{A.24}$$

The solution $\{u\}$ corresponds to a resulting load $P = P_c(1+\kappa)$ with eccentricity $m = e/d = (0.5 + \kappa m_{td})/(1+\kappa)$.

Appendix B. Uniqueness and superposition at dissipative friction

If $[\mathbf{r}]$, $\sigma_0 = 0$ and $\beta = 0$ there applies the following proposition.

Proposition B.1. *If complementarity prevails and to load p^*, u^* there corresponds a solution $\{\sigma, u\}$, this solution is unique provided either the normal stress σ or the slip deformation $\boldsymbol{\gamma}_t$ is prescribed on every contact surface Γ_c where $\gamma_n = 0$.*

Proof. The proof follows the procedure in the proof of Theorem 1 (Part I). Let us consider two solutions $\{\sigma^1, u^1\}$, $\{\sigma^2, u^2\}$. Then, because of complementarity according to Eq. (52b, Part I), there holds

$$a(u^2 - u^1, u^2 - u^1) + \langle p^2 - p^1, \gamma^2 - \gamma^1\rangle_{\partial H} = 0 \tag{B.1a}$$

where $a(u^2 - u^1, u^2 - u^1)$ is positive definite and the second term can be expressed by

$$\langle p^2 - p^1, \gamma^2 - \gamma^1\rangle_{\partial H} = \langle \tau^2 - \tau^1, \gamma_t^2\rangle + \langle \tau^1 - \tau^2, \gamma_t^1\rangle + \langle \sigma^2 - \sigma^1, \gamma_n^2\rangle + \langle \sigma^1 - \sigma^2, \gamma_n^1\rangle \tag{B.1b}$$

or alternatively by

$$\langle p^2 - p^1, \gamma^2 - \gamma^1\rangle_{\partial H} = \langle \tau^2, \gamma_t^2 - \gamma_t^1\rangle + \langle \tau^1, \gamma_t^1 - \gamma_t^2\rangle + \langle \sigma^2, \gamma_n^2 - \gamma_n^1\rangle + \langle \sigma^1, \gamma_n^1 - \gamma_n^2\rangle \tag{B.1c}$$

Because stresses and deformations are admissible they are subjected to the sectional normality rule (Eq. (20), Part I)

$$\boldsymbol{\gamma}_{\mathrm{t}}^{i} \cdot (\boldsymbol{\tau}^{i}/|\sigma^{i}| - \boldsymbol{\tau}^{j}/|\sigma^{j}|) \geqslant 0; \quad i,j = \{1,2\} \tag{B.2}$$

If $\sigma^1 = \sigma^2$ is prescribed on Γ_{c} then the left hand side of Eq. (B.1b) becomes nonnegative because of Eq. (B.2). If again we prescribe $\gamma_{\mathrm{t}}^1 = \gamma_{\mathrm{t}}^2$ where $\gamma_{\mathrm{n}}^1 = \gamma_{\mathrm{n}}^2 = 0$ the expression (B.1c) equals zero. Because $a(u^2 - u^1, u^2 - u^1)$ is positive definite, the left hand side of Eq. (B.1a) becomes nonnegative from which there follows $\{\sigma^1, u^1\} = \{\sigma^2, u^2\}$. □

The following superposition rule applies irrespective of the kind of friction.

Lemma B.1. *If load $\{p^{1*}, u^{1*}\}$ induces a state $\{\sigma^1, u^1\}$ with actual contact interfaces $\cup\Gamma_c$ and load $\{p^{2*}, u^{2*}\}$ induces a state $\{\sigma^2, u^2\}$ with the same contact interfaces $\cup\Gamma_c$, then the load $\{p^*, u^*\} = \{p^{1*} + p^{2*}, u^{1*} + u^{2*}\}$ induces a state $\{\sigma, u\} = \{\sigma^1 + \sigma^2, u^1 + u^2\}$ with unchanged interfaces $\cup\Gamma_c$, provided that either γ^1, γ^2 or τ^1, τ^2 vanish identically on $\cup\Gamma_c$.*

The lemma follows immediately from the correspondence rule and by application of Eq. (B.1a) to the expression $a(u - (u^1 + u^2), u - (u^1 + u^2))$.

Lemma B.2. *If a dry joint $\Gamma_{\nu\mu}$ constitutes a plane of symmetry in a sufficiently large part $\Delta\Omega$ of the structure an external load p^* acting on $\Delta\Omega$ can be decomposed into a symmetric part p_s^* and an antisymmetric part p_a^*. Then the region of actual contact is determined uniquely by p_s^*, being independent of p_a^* (Kalker, 1990).*

Proof. Let a detachable joint $\Gamma_{\nu\mu}$ in the structure constitute a plane yz of symmetry with normal in direction x. A symmetric load p_{s}^* will then induce a symmetrical state $\{\sigma, u\}_{\mathrm{s}}$ where the change in distance between symmetrically situated points is $\Delta u_{x\mathrm{s}} = u_{x\mathrm{s}}(\mathrm{x}) - u_{x\mathrm{s}}(-x) = 2u_{x\mathrm{s}}(x)$. If we add to p_{s}^* an antisymmetrical load p_{a}^* and either $\gamma_{\mathrm{ta}} = 0$ or $\beta = 0$ on $\Gamma_{\nu\mu}$, this will induce an additional antisymmetrical state $\{\sigma, u\}_{\mathrm{a}}$ where the distance between symmetrically situated points does not change $\Delta u_{x\mathrm{a}} = u_{x\mathrm{a}}(x) - u_{x\mathrm{a}}(-x) = 0$ and the contact region remains unchanged $\Gamma_{\mathrm{ca}} = \Gamma_{\mathrm{cs}}$. The load $p^* = p_{\mathrm{s}}^* + p_{\mathrm{a}}^*$ induces a state $\{\sigma, u\}$ to which applies the superposition rule

$$\{\sigma, u\} = \{\sigma, u\}_{\mathrm{s}} + \{\sigma, u\}_{\mathrm{a}} \tag{B.3}$$

This follows directly from Proposition B.1, Lemma B.1 and the noncommutative superposition of $\{\sigma, u\}_{\mathrm{s}}$ and $\{\sigma, u\}_{\mathrm{a}}$. □

References

Gladwell, G., 1980. Contact problems in the classical theory of elasticity. Sijthoff and Noordhoff, Alphena.

Kalker, J.J., 1990. Three-dimensional elastic bodies in rolling contact. Kluwer Academic Publishers, Dordrecht.

Miettinen, A., 1988. Ulokesauman kitka ja sen teoria (in Finnish). In: Ranta, M. (Ed.), Proceedings of the Third Finnish Mechanics Days. Helsinki University of Technology, pp. 219–228.

Parland, H., 1995. Dilatational effects in nonmonolithic structures. In: Proceedings of the Second Contact Mechanics International Symposium. Plenum Press, New York.

Parland, H., Miettinen, A., 1985. Linear and nonlinear contact problems. In: Proceedings of the International Conference on Nonlinear Mechanics 1985, Shanghai. Science Press, Beijing.